Sea Surface Temperature Biases under the Stratus Cloud Deck in the Southeast Pacific Ocean in 19 IPCC AR4 Coupled General Circulation Models

YANGXING ZHENG*

Cooperative Institute for Research in Environmental Sciences, University of Colorado, Boulder, Colorado

TOSHIAKI SHINODA

Naval Research Laboratory, Stennis Space Center, Mississippi

JIA-LIN LIN

Department of Geography, The Ohio State University, Columbus, Ohio

GEORGE N. KILADIS

NOAA/Earth System Research Laboratory/Physical Science Division, Boulder, Colorado

(Manuscript received 27 October 2010, in final form 27 January 2011)

ABSTRACT

This study examines systematic biases in sea surface temperature (SST) under the stratus cloud deck in the southeast Pacific Ocean and upper-ocean processes relevant to the SST biases in 19 coupled general circulation models (CGCMs) participating in the Intergovernmental Panel on Climate Change (IPCC) Fourth Assessment Report (AR4). The 20 years of simulations from each model are analyzed. Pronounced warm SST biases in a large portion of the southeast Pacific stratus region are found in all models. Processes that could contribute to the SST biases are examined in detail based on the computation of major terms in the upper-ocean heat budget. Negative biases in net surface heat fluxes are evident in most of the models, suggesting that the cause of the warm SST biases in models is not explained by errors in net surface heat fluxes. Biases in heat transport by Ekman currents largely contribute to the warm SST biases both near the coast and the open ocean. In the coastal area, southwestward Ekman currents and upwelling in most models are much weaker than observed owing to weaker alongshore winds, resulting in insufficient advection of cold water from the coast. In the open ocean, warm advection due to Ekman currents is overestimated in models because of the larger meridional temperature gradient, the smaller zonal temperature gradient, and overly weaker Ekman currents.

1. Introduction

Climate in the southeast Pacific (SEP) near the coast of Peru and Chile is controlled by complex upper-ocean, marine boundary layer and land processes and their interactions. A variety of coupled processes between the ocean and atmosphere are involved in this tightly coupled system, and the variation of the system has significant impacts on global climate (e.g., Ma et al. 1996; Miller 1997; Gordon et al. 2000; Xie 2004). For example, strong winds parallel to the coast generate intense coastal upwelling, bringing cold water to the ocean surface, which helps to maintain the persistent stratus/stratocumulus cloud decks by stabilizing the lower troposphere. These persistent stratus decks have a substantial impact on the surface energy budget in the tropics and subtropics by reflecting sunlight back to space.

It is well known that coupled atmosphere–ocean general circulation models (GCMs) tend to have systematic errors in the SEP region, including a warm bias in SST and too little cloud cover (e.g., Mechoso et al.

* Current affiliation: The Florida State University, Tallahassee, Florida.

Corresponding author address: Yangxing Zheng, Center for Ocean–Atmospheric Prediction Studies, The Florida State University, 2035 E. Paul Dirac Dr., Johnson Building, Tallahassee, FL 32306-2840.
E-mail: yzheng@fsu.edu

DOI: 10.1175/2011JCLI4172.1

1995; Ma et al. 1996; Gordon et al. 2000; McAvaney et al. 2001; Kiehl and Gent 2004; Large and Danabasoglu 2006; Wittenberg et al. 2006; Lin 2007). These biases have important impacts on the simulated earth's radiation budget and climate sensitivity. Also, the accurate prediction of low clouds over the SEP is required to simulate the proper strength of the trade winds and the observed SST distribution in the tropics (Ma et al. 1996; Gordon et al. 2000).

Although the previous studies described above reported a warm SST bias in the SEP region in many coupled GCMs (CGCMs), it is still uncertain whether a similar bias is evident in most state-of-the-art CGCMs and to what extent the SST biases are model dependent. Recently, in preparation for the Intergovernmental Panel on Climate Change (IPCC) Fourth Assessment Report (AR4), many international climate modeling centers conducted a comprehensive set of climate simulations for the twentieth century's climate and different climate change scenarios in the twenty-first century. The release of the output of IPCC AR4 CGCM simulations provided an opportunity to investigate the systematic biases in the SEP region using long-term simulations with a variety of CGCMs. Recently, de Szoeke and Xie (2008) found a warm SST error on the equator near the South American coast (2°S–2°N, 90°–80°W) in the IPCC AR4 CGCM simulations and attributed the error to a weaker meridional wind compared to observations. In this study, we will quantify systematic SST biases in the SEP region in these IPCC AR4 CGCM simulations and attempt to isolate their causes.

Since the SEP climate is a tightly coupled system, inaccurate simulations of both atmospheric and oceanic processes and their interactions may contribute to the SST biases. Accordingly, it is necessary to examine individual biases in the OGCMs) and the atmospheric GCMs (AGCMs), along with the biases in the accompanying ocean–atmosphere feedback processes so as to provide useful guidance on how to improve the CGCM simulations. The importance of three-dimensional upper-ocean processes for controlling SST in the SEP region has been recently demonstrated by observations, and OGCM and CGCM experiments (Colbo and Weller 2007; Shinoda and Lin 2009; Zheng et al. 2010; Toniazzo et al. 2010). For example, Zheng et al. (2010) estimated the annual mean heat budget using eddy-resolving OGCM experiments and indicated the dominant role of horizontal advection of upwelled cold water from the coast in balancing the positive surface heat flux and thus maintaining the annual mean SST in the SEP region. Using regional model simulations in the SEP, McWilliams and Colas (2010) and F. Colas et al. (2011, personal communication) argue that the oceanic warming from surface heat fluxes off Peru and Chile (700 km from the coastline) is balanced by cooling associated with lateral heat transport by both mean currents and eddies from the coastal upwelling zone. Hence, the accurate simulation of upper-ocean processes as well as air–sea fluxes is crucial for correctly simulating SST in this region.

Deficiencies in simulating upper-ocean processes in the SEP region have been found in some CGCM experiments. For example, Large and Danabasoglu (2006) examined the largest and potentially most important ocean near-surface biases in the Community Climate System Model, version 3 (CCSM3), coupled simulation of present-day conditions. The largest mean SST biases develop along the eastern boundaries of subtropical gyres, including the SEP region, and the overall coupled model response is found to be linear. Based on the subsequent ocean-only experiment, they suggested that the cause of the warm bias in the southeastern tropical oceans could be traced back to inadequate coastal upwelling close to the coast; that is, at least part of the cause was contained in the ocean model.

Attribution of SST errors was recently investigated by de Szoeke et al. (2010) for October climatology along 20°S from 85° to 75°W in 15 IPCC AR4 CGCMs using ship observations and three gridded observation-based surface heat flux datasets. They found that solar radiation and evaporation at the surface are overestimated in IPCC GCMs during this season. A major focus of the present study is to identify upper-ocean processes and surface fluxes in the entire SEP region that could be relevant to SST warm biases in CGCMs. Although the data coverage of in situ observations in the upper ocean and air–sea fluxes in the SEP region are still sparse, global datasets of surface fluxes [e.g., the objectively analyzed air–sea fluxes (OAFlux), Yu and Weller (2007)] and ocean analysis [e.g., the Simple Ocean Data Assimilation (SODA), Carton and Giese (2008)] have been significantly improved in recent years because a variety of satellite data are used in the analyses. Hence, it is now feasible to evaluate the ability of CGCMs to simulate air–sea fluxes and upper-ocean currents and temperature compared to reasonable estimates of some quantities from the real world. In this study, we will examine errors in upper-ocean processes and surface fluxes in CGCMs that could contribute to the biases in SST. Major terms in the upper-ocean heat budget are estimated using the output of CGCMs, and they are compared with those from the ocean analysis and surface flux estimates based on satellite measurements. Submesoscale eddies are not resolved in all IPCC AR4 CGCMs, which might impact SST biases in these models. The possible impact of resolving eddies in these models on the SST biases is discussed based on recent studies that include the analysis of the data from the Variability of the American Monsoon

TABLE 1. List of the 19 IPCC AR4 coupled GCMs that participated in the study.

Modeling Groups	IPCC identifier (label in figures)	Resolution[a] (stratus)[b]	Heat flux correction	Run
Bjerknes Center for Climate Research	BCCR-BCM2.0 (bccr)	360 × 180-L33 (1 × 1)	None	1
Canadian Centre for Climate Modelling and Analysis	CGCMA3.1-T47 (cgcm-t47)	192 × 96-L29 (1.9 × 1.9)	Yes	1
Canadian Centre for Climate Modelling and Analysis	CGCMA3.1-T63 (cgcm-t63)	256 × 192-L29 (1.4 × 0.93)	Yes	1
Météo-France/Centre National de Recherches Météorologique	CNRM-CM3 (cnrm)	180 × 170-L33 (2 × 1)	None	1
Commonwealth Scientific and Industrial Research Organisation (CSIRO) Marine and Atmospheric Research	CSIRO Mk3.0 (csiro mk3.0)	192 × 189 × L31 (1.9 × 0.93)	None	2
CSIRO Marine and Atmospheric Research	CSIRO Mk3.5 (csiro mk3.5)	192 × 189 × L31 (1.9 × 0.93)	None	1
NASA Goddard Institute for Space Studies	GISS-AOM (giss-aom)	90 × 60-L31(4 × 3)	None	1
NASA Goddard Institute for Space Studies	GISS-ER (giss-er)	72 × 46-L33 (5 × 4)	None	1
State Key Laboratory of Numerical Modeling for Atmospheric Sciences and Geophysical Fluid Dynamics (LASG), Institute of Atmospheric Physics	FGOALS-g1.0 (iap)	360 × 170-L33 (1 × 1)	None	1
Instituto Nazionale di Geofisica e Vulcanologia	INGV-SXG (ingv)	360 × 180-L33 (1 × 1)	None	1
L'Institut Pierre-Simon Laplace	IPSL CM4 (ipsl)	180 × 170-L31(2 × 1)	None	1
Center for Climate System Research (The University of Tokyo), National Institute for Environmental Studies, and Frontier Research Center for Global Change	MIROC3.2(hires) (miroc-hires)	320 × 320-L33 (1.1 × 0.56)	None	1
Center for Climate System Research (The University of Tokyo), National Institute for Environmental Studies, and Frontier Research Center for Global Change	MIROC3.2(medres) (miroc-medres)	256 × 192-L33 (1.4 × 0.93)	None	2
Max Planck Institute for Meteorology	ECHAM5/MPI-OM (mpi)	360 × 180-L40 (1 × 1)	None	1
Meteorological Research Institute	MRI CGCM2.3.2 (mri)	144 × 111-L23(2.5 × 2)	Yes[c]	1
National Center for Atmospheric Research	CCSM3 (ccsm3)	320 × 395-L40 (1.1 × 0.27)[d]	None	1
National Center for Atmospheric Research	PCM (pcm)	360 × 180-L32 (1 × 1)	None	3
Met Office Hadley Centre for Climate Change	UKMO-HadCM3 (hadcm3)	288 × 144-L20 (1.25 × 1.25)	None	1
Met Office Hadley Centre for Climate Change	UKMO-HadGEM1 (hadgem1)	360 × 216-L40 (1 × 0.7)[d]	None	1

[a] Resolution is about ocean model output, which is denoted by number of grid points (longitude × latitude) and of vertical layers (L).
[b] Parenthesis shows horizontal resolution (longitude × latitude) in degrees around the stratus region (35°–5°S, 100°–70°W).
[c] Monthly climatological flux adjustment for heat (only 12°S–12°N) is used.
[d] Grid points are not even in latitude; resolution in latitude is finer as it gets closer to the equator.

Systems (VAMOS) Ocean–Cloud–Atmosphere–Land Study Regional Experiment (VOCALS Rex).

2. Models and validation datasets

a. IPCC models

The analysis is based on 20-yr (1980–99) model runs of the Climate of the Twentieth Century (20C3M) simulations from 19 coupled GCMs. Table 1 shows the model names and acronyms, their ocean model horizontal and vertical resolutions, heat flux corrections, and which run is employed for analysis. The resolution of the ocean models within the stratus region is also shown. For each model, we use 20 years of monthly mean ocean temperature, salinity, three-dimensional ocean currents, surface wind stress, sea level pressure, surface downward/upward shortwave/longwave radiation, surface latent heat flux, surface sensible heat flux, and near-surface meteorological variables (wind speed at 10 m, and air temperature and air specific humidity at 2 m).

b. SODA

The SODA methodology, the ingested data, and the error covariance structure of both the model and the observations are described by Carton et al. (2000a,b), Carton and Giese (2008), and Zheng and Giese (2009). The ocean model is based on the Los Alamos implementation of the Parallel Ocean Program (POP) (Smith et al. 1992). The model resolution is on average 0.25° latitude × 0.4° longitude with 40 levels in the vertical. The model is forced with the 40-yr European Centre for Medium-Range Weather Forecasts Re-Analysis (ERA-40) daily atmospheric reanalysis winds (Simmons and Gibson 2002) for the 44-yr period from 1958 to 2001.

Surface heat fluxes are computed from bulk formulae (Smith et al. 1992), with atmospheric variables from the National Centers for Environmental Prediction–National Center for Atmospheric Research (NCEP–NCAR) reanalysis (Kalnay et al. 1996). The NCEP–NCAR reanalysis information is used for the bulk formulae instead of the ERA-40 variables throughout the experiment to give continuity of surface forcing during periods for which the ERA-40 winds are not available. However, the details of surface heat flux boundary condition are relatively unimportant in influencing the solution since near-surface temperature observations are used to update the mixed layer temperature. Vertical diffusion of momentum, heat, and salt is based on a nonlocal *K*-profile parameterization (KPP) (Large et al. 1994), and horizontal diffusion for subgrid-scale processes is based on a biharmonic mixing scheme.

The model is constrained by observed temperature and salinity using a sequential assimilation algorithm, which is described by Carton et al. (2000a,b) and Carton and Giese (2008). The basic subsurface temperature and salinity observation sets consist of approximately 7×10^6 profiles of which two-thirds have been obtained from the *World Ocean Atlas 2001* (Boyer et al. 2002; Stephens et al. 2002) with online updates through December 2004. This dataset has been extended by the addition of real-time temperature profile observations from the Tropical Atmosphere Ocean/Triangle Trans-Ocean Buoy Network (TAO/TRITON) mooring thermistor array and Argo floats. In addition to the temperature profile data, a large number of near-surface temperature observations are available, both in the form of in situ measurements [bucket and ship-intake temperatures from the Comprehensive Ocean–Atmosphere Data Set (COADS) surface marine observation set of Diaz et al. (2002)] and from satellite remote sensing. SODA used the nighttime NOAA–National Aeronautics and Space Administration (NASA) Advanced Very High Resolution Radiometer (AVHRR) operational SST data, which began November 1981 and averages 25 000 samples per week. Use of only nighttime retrievals reduces the error due to skin temperature effects. However, the biggest challenge in retrieving SST from an IR instrument in the southeast Pacific Ocean is the cloud detection problem since clouds are opaque to infrared radiation and can effectively mask radiation from the ocean surface. Carton et al. (2000a,b) used a bias-corrected model error covariance in an attempt to reduce such error. The near-surface salinity observation set averages more than 10^5 observations per year since 1960 (Bingham et al. 2002). Nearly continuous sea level information is available from a succession of altimeter satellites beginning in 1991. Although the coverage of subsurface data in the southeast Pacific Ocean is not as good as in other regions of the tropics, a significant amount of satellite observations are used in SODA, especially after 1980 (not shown). The yearly number of observations in the southeast Pacific (35°–5°S, 140°–70°W) exceeds 10^5 after 1984. Hence, it is likely that the SODA analysis can provide more accurate estimates of mean heat advection than models with no data assimilation. In fact, temperature and ocean surface currents are reasonably good when compared to *World Ocean Atlas 2005* (*WOA05*) monthly climatology and near-real-time ocean surface currents derived from satellite altimeter and scatterometer data [i.e., Ocean Surface Current Analyses—Real Time (OSCAR) products; see http://www.oscar.noaa.gov/ (not shown)]. Furthermore, horizontal heat advection in SODA is comparable to those derived from other independent datasets, such as *WOA05* and the NCEP Pacific Ocean analysis (see the appendix). The consistency between SODA and other datasets indicates that SODA is suitable for this study provided that there are no better alternatives.

Averages of model output variables (temperature, salinity, and velocity) are saved at 5-day intervals. These average fields are remapped onto a uniform global $0.5° \times 0.5°$ horizontal grid using the *horizontal-grid spherical coordinate remapping and interpolation package* with second-order conservative remapping (Jones 1999).

c. Heat flux datasets

In this study, monthly mean surface fluxes from OAFlux (Yu and Weller 2007; Yu et al. 2008) are primarily used for evaluating the biases of heat fluxes in CGCMs since they are the latest—and perhaps the best—validated datasets. Near-surface meteorological variables and SST used to estimate the fluxes are obtained from an optimal blending of satellite retrievals and two versions of NCEP reanalyses [i.e., NCEP–NCAR Global Reanalysis 1 (NCEP-1) and Reanalysis 2 (NCEP-2)] and ERA-40. NCEP-1 represents the NCEP–NCAR reanalysis project that has produced an ongoing dataset from 1948 to the present (Kalnay et al. 1996), and NCEP-2 represents the NCEP–DOE reanalysis project in an effort to correct known errors in NCEP-1 from 1979 to the present and to improve parameterizations of some physical processes (Kanamitsu et al. 2002). The latent and sensible fluxes are computed from the optimally estimated near-surface atmospheric variables and SST using the Tropical Ocean and Global Atmosphere Coupled Ocean–Atmosphere Response Experiment (TOGA COARE) bulk air–sea flux algorithm, version 3.0 (Fairall et al. 2003). Surface latent and sensible heat fluxes as well as meteorological variables near the surface are available from January 1958 to December 2008. Surface shortwave and longwave radiation of OAFlux is derived from the International

TABLE 2. List of monthly observational datasets used in this study.

Variables	Dataset	Spatial coverage/resolution (°)	Temporal coverage	Reference
Ocean temperature and salinity	SODA	Global ocean 0.5 × 0.5-L40	Jan 1958–Dec 2005	Carton and Giese (2008)
	WOA05	Global ocean 1 × 1-L24	Monthly climatology	Locarnini et al. (2006) Antonov et al. (2006)
Ocean velocity	SODA	Global ocean 0.5 × 0.5-L40	Jan 1958–Dec 2005	Carton and Giese (2008)
Surface wind stress	ERA-40	Global ocean 0.5 × 0.5	Jan 1958–Dec 2001	Simmons and Gibson (2002)
Net surface heat flux	OAFlux	Global ocean 1 × 1	Jul 1983–Dec 2007	Yu and Weller (2007)
	NCEP-1	Global ocean 1.9 × 1.9	Jan 1948–present	Kalnay et al. (1996)
	NCEP-2	Global ocean 1.9 × 1.9	Jan 1979–Dec 2008	Kanamitsu et al. (2002)
	ERA-40	Global ocean 2.5 × 2.5	Sep 1957–Aug 2002	Uppala et al. (2005)
Surface latent/sensible heat flux	OAFlux	Global ocean 1 × 1	Jan 1958–Dec 2008	Yu and Weller (2007)
	GSSTF2	Global ocean 1 × 1	Jan 1988–Dec 2000	Chou et al. (2003)
Net surface shortwave/ longwave flux	ISCCP-FD	Global ocean 1 × 1	Jul 1983–Dec 2007	Rossow et al. (1996) Yu and Weller (2007)
Air temperature at 2 m	OAFlux	Global ocean 1 × 1	Jan 1958–Dec 2008	Yu and Weller (2007)
Sea surface skin temperature	OAFlux	Global ocean 1 × 1	Jan 1958–Dec 2008	Yu and Weller (2007)
Air specific humidity at 2 m	OAFlux	Global ocean 1 × 1	Jan 1958–Dec 2008	Yu and Weller (2007)
Wind speed at 10 m	OAFlux	Global ocean 1 × 1	Jan 1958–Dec 2008	Yu and Weller (2007)

Satellite Cloud Climatology Project flux dataset (ISCCP-FD) estimates (Zhang et al. 2004) that are available from 1 July 1983. These flux estimates are compared to 107 (105 buoys and two ships) in situ flux time series, and found to be relatively unbiased and have the smallest mean error compared to other datasets (Yu and Weller 2007; Yu et al. 2008).

Since there are still significant uncertainties in surface heat flux estimates (e.g., Kubota et al. 2003; Brunke et al. 2003; Chou et al. 2004; Yu et al. 2008), we also use monthly mean heat fluxes from NCEP-1, NCEP-2, ERA-40, and the Goddard Satellite-Based Surface Turbulent Fluxes Version 2 (GSSTF2) for the evaluation of model surface fluxes. Latent and sensible heat fluxes in GSSTF2 are estimated from satellite-derived meteorological variables and SST with a bulk flux algorithm, including salinity and cool-skin effects (Chou et al. 2003). Observational datasets and an ocean analysis dataset used for evaluating the model simulations are summarized in Table 2.

3. SST biases

Figure 1 shows the spatial distribution of SST biases in the southeast Pacific Ocean (35°–5°S, 100°–70°W) from 19 IPCC AR4 coupled GCMs along with the mean SST averaged from *WOA05* monthly climatology (Antonov et al. 2006; Locarnini et al. 2006) (shown in top left panel). The SST biases are computed as the difference between the model SST averaged over the period 1980 through 1999 and *WOA05* SST. Warm biases in SST are evident in most models, especially in the northern part of the stratus region, with the greatest values near the coast, except in the INGV and the MPI models in which peak values are offshore. The warm SST biases are generally weaker in the southern part of the stratus region, and cold biases are found in some models. These latitudinal variations of SST biases are further shown in the SST biases averaged along 100°–70°W as a function of latitude (Fig. 2). Most models have warm SST biases north of 20°S. The magnitude of the bias varies substantially from model to model, especially around 5°S (~0°–5°C). It should be noted that relatively small values of SST biases in the MRI CGCM-T47 and MRI CGCM-T63 are likely to be due to the heat flux corrections (Table 1).

4. Surface heat fluxes and upper-ocean processes

Errors in both surface heat fluxes and upper-ocean processes such as horizontal advection and upwelling could contribute to the warm SST biases in models. In this section, we evaluate biases in surface heat fluxes and major terms in the heat equation in models based on the comparison with those from surface flux datasets and SODA described in section 2. Since large SST biases are found mostly in the northern part of the stratus region, the analysis is performed for the region north of 20°S.

a. Surface fluxes

1) NET SURFACE HEAT FLUXES

Figure 3 shows the biases of net surface heat fluxes from 17 IPCC AR4 coupled GCMs relative to the net surface heat fluxes from OAFlux (top left panel) that were averaged over the period July 1983–December 1999. Note that two models (i.e., INGV and PCM) are not included here because surface shortwave and longwave fluxes from these models are not available. Also,

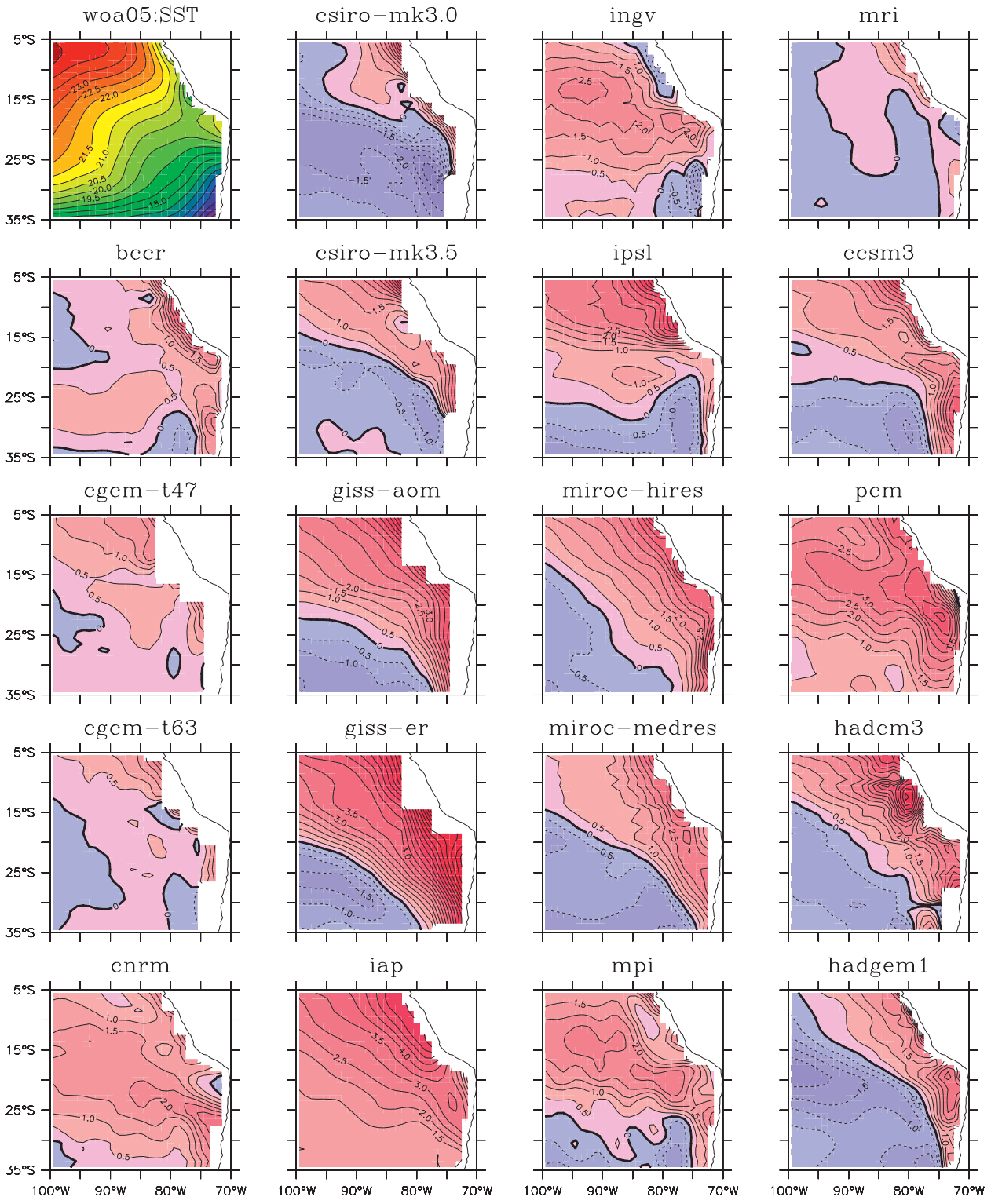

FIG. 1. Spatial distribution of the SST biases (shading contours; °C) relative to *WOA05* from 19 IPCC AR4 coupled GCMs in the region (35°–5°S, 100°–70°W): (top left) SST from *WOA05*. Contour interval is 0.5°C.

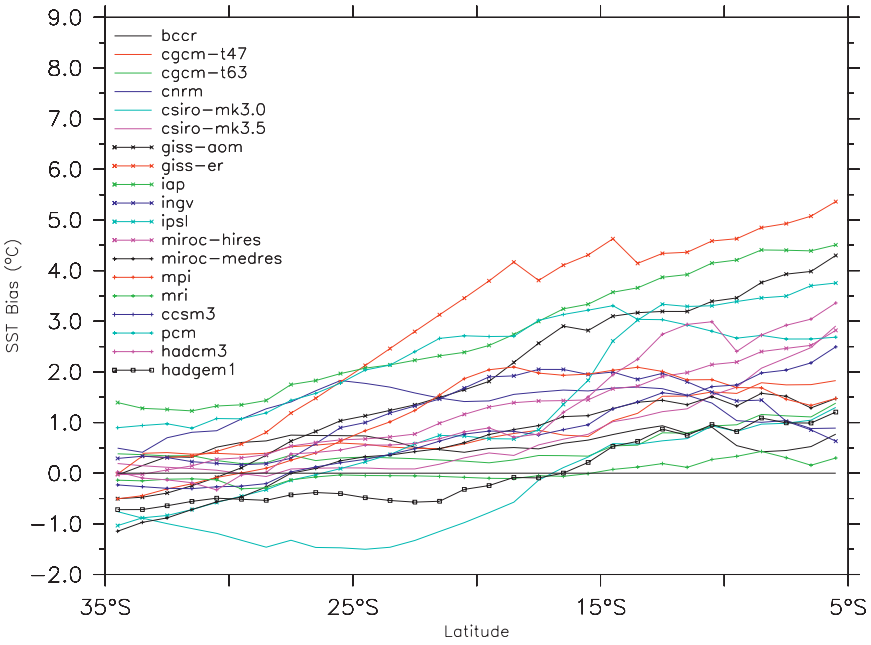

FIG. 2. Biases of SST (°C) in the 19 IPCC AR4 coupled GCMs, zonally averaged along 100°–70°W as a function of latitude in the southeast Pacific Ocean. SST biases are computed relative to *WOA05* monthly climatology temperature datasets. The model period for computing model SST biases is January 1980–December 1999.

note that radiation from ISCCP-FD (and thus net surface fluxes from OAFlux) is available only from 1 July 1983. The net surface heat fluxes from OAFlux are positive (warming the ocean, positive downward) in the entire region of the analysis with the magnitude ~50–120 W m^{-2}. All models have negative biases of the net surface heat fluxes (i.e., insufficiently warming the ocean) in almost the entire region of the analysis. Our result is consistent with de Szoeke et al. (2010), who compared the estimate of surface fluxes from VOCALS Rex (along 20°S in October) with those from IPCC AR4 CGCMs, in which negative biases in net surface heat flux are found (Fig. 10 in their paper). Positive biases are found in small regions near the coastline in some models. The nearly universal cold biases in net surface heat fluxes suggest that the warm SST biases in the models are not primarily caused by errors in net surface heat fluxes.

2) INDIVIDUAL COMPONENTS OF SURFACE HEAT FLUXES

Biases in each component of surface heat fluxes are further examined to identify which component contributes most to negative biases of the net surface heat fluxes in CGCMs. Figure 4 displays the biases (denoted by "×") of surface latent and sensible heat fluxes, shortwave and longwave radiation (LHF, SHF, SW, and LW, respectively), and net surface heat fluxes averaged over the area (20°–5°S, 100°–70°W). The horizontal lines denote zero biases. The biases of these components are relative to LHF and SHF from OAFlux and SW and LW from ISCCP-FD during July 1983–December 1999. Note that positive (negative) values in all components indicate warming (cooling) of the ocean. The major components contributing to negative net surface heat flux biases are LHF and LW. Positive biases in SW are evident in most models, indicating too few stratus clouds over this region (e.g., Lin 2007). Thus, biases in SW would contribute to warm SST biases in the models. However, negative biases in LW, LHF, and SHF are found in all models: the summation of these negative biases exceeds the amount of positive biases in SW, resulting in negative biases in the net surface heat flux.

Negative biases of LHF and SHF could stem from the errors of near-surface meteorological variables and SST as well as the use of different bulk flux algorithms. Figure 5 shows biases of near-surface meteorological variables averaged over the area (20°–5°S, 100°–70°W). The specific humidity (qa) is larger and wind speed (ws) is smaller in most models than those from OAFlux (Figs. 5a and 5d), which results in smaller ws(qs − qa) (Fig. 5e). Hence, errors in near-surface meteorological variables do not cause negative biases in LHF. Similarly, ws(SST − T_a) is smaller than that from OAFlux in most models (Fig. 5f); thus errors in near-surface meteorological variables do not cause negative biases in SHF. Since errors of individual components of heat fluxes are pronounced—particularly

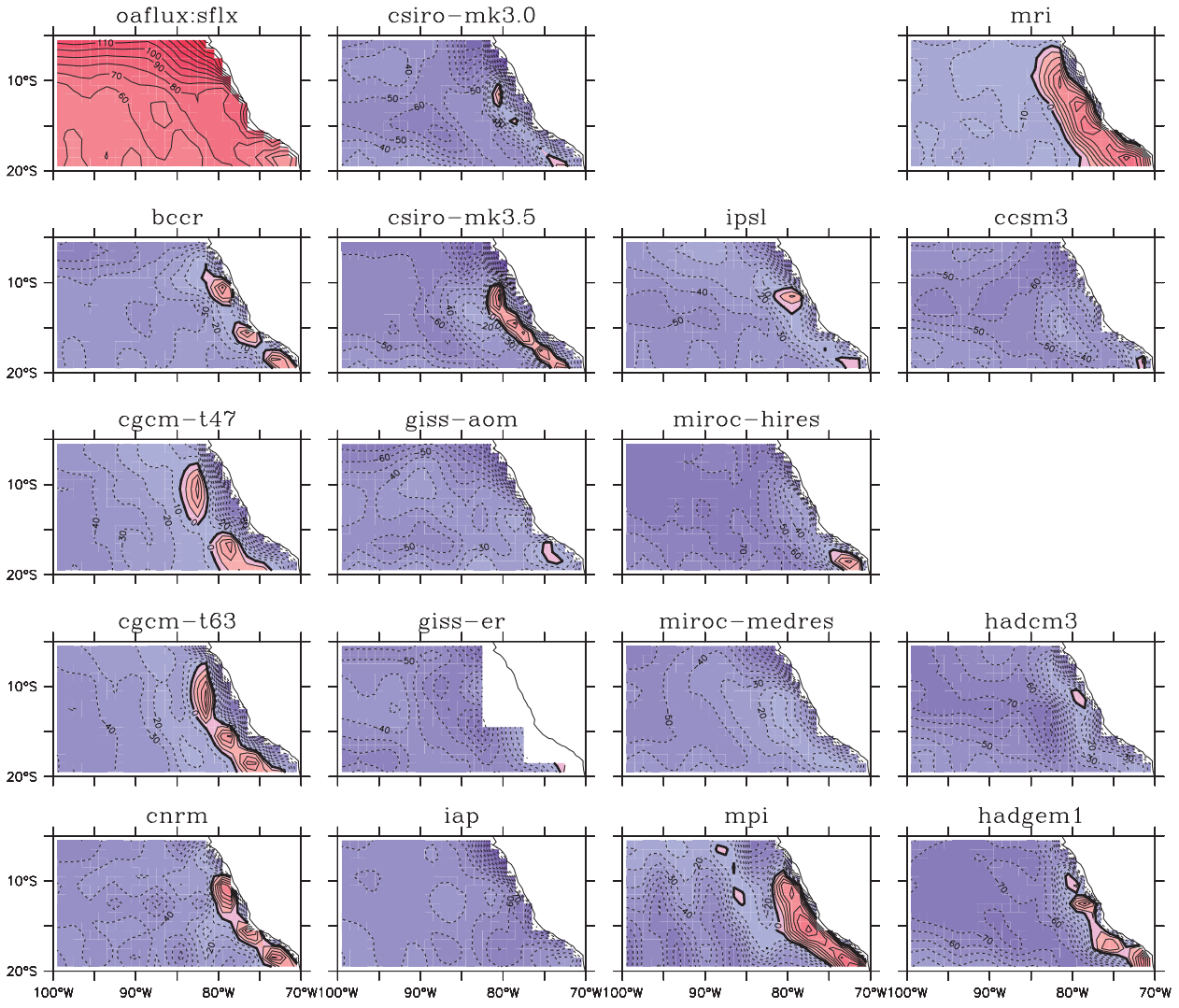

FIG. 3. Spatial distribution of the net surface heat flux biases (shading contours; W m^{-2}) relative to OAFlux from 17 IPCC AR4 coupled GCMs in the region (20°–5°S, 100°–70°W) of the SEP: (top left) net surface heat flux from OAFlux.

the errors in the latent heat flux, shortwave and longwave radiation due to a lack of clouds, and too high SST in models—they will contribute to SST biases in IPCC models, though the modeled net surface heat fluxes appear to be insufficient to generate warm SST biases.

3) COMPARISON WITH OTHER SURFACE FLUX DATASETS

Although OAFlux estimates are relatively well validated, it is difficult to determine their uncertainties because of very few in situ observations of surface fluxes in the SEP region. To further confirm the negative biases in model heat fluxes, we compared model fluxes with other surface flux datasets. Net surface heat fluxes from NCEP-1, NCEP-2, and ERA-40 are used for the comparison. In addition to these reanalysis datasets, satellite-based latent and sensible heat fluxes (GSSTF2) and radiation (ISCCP-FD) are also used. Figure 6 shows the biases of net surface heat flux averaged over the region (20°–5°S, 100°–70°W) relative to the five datasets over the period January 1988–December 1999. While there are significant differences between the datasets, negative biases are found in all models except MRI, suggesting that our results on surface heat flux biases are robust—at least qualitatively.

b. Upper-ocean processes

Zheng et al. (2010) indicated that three-dimensional upper-ocean processes, such as horizontal heat advection, play an important role in controlling the annual mean SST in the stratus region based on the computation of upper-ocean heat budget using OGCM experiments.

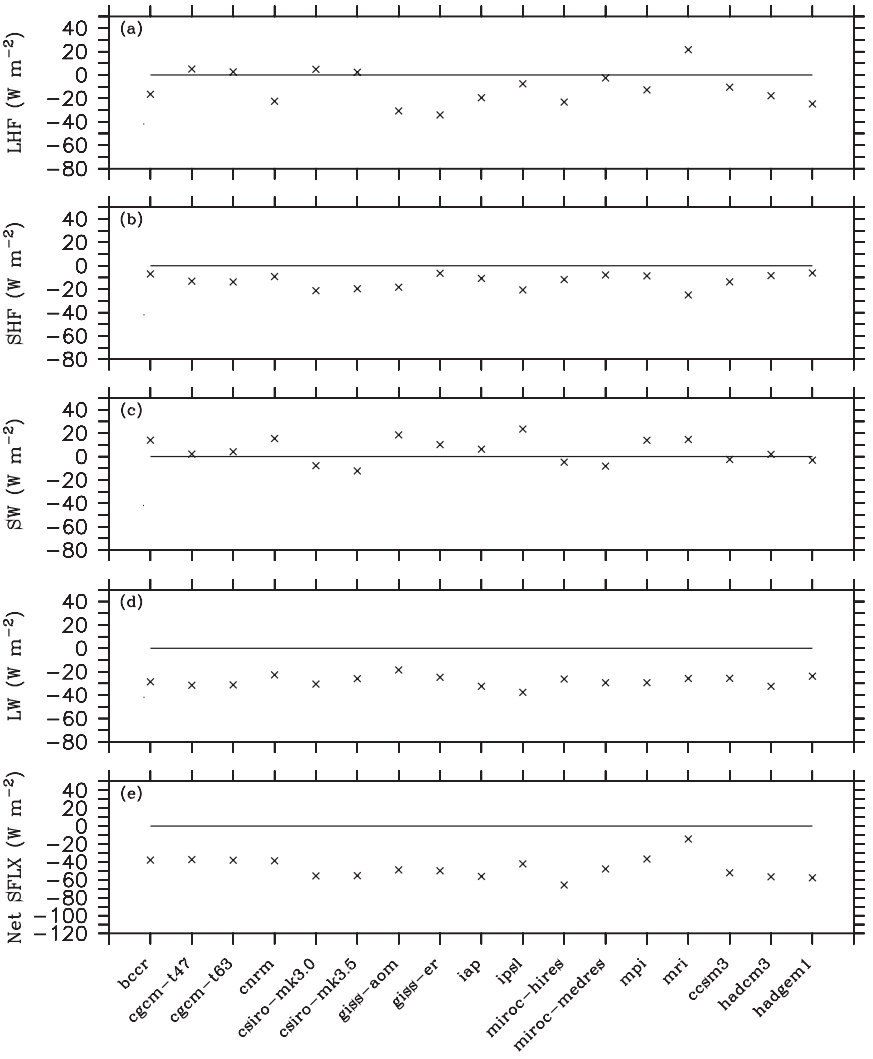

FIG. 4. Biases of (a) LHF, (b) SHF, (c) net SW and (d) net LW at the ocean surface, and (e) net surface heat flux from 17 IPCC AR4 coupled GCMs averaged in 20°–5°S, 100°–70°W: all fluxes and radiation (W m^{-2}). Biases are computed relative to the OAFlux monthly estimates during July 1983–December 1999. Horizontal lines denote zero biases.

Analyses similar to those in Zheng et al. are performed using the IPCC model outputs to examine the impact of errors in upper-ocean processes on the SST biases.

1) HORIZONTAL HEAT ADVECTION

Horizontal heat advection integrated from the surface to the depth z_0 is defined as

$$H_{\text{adv}} = -\int_{z_0}^{0} \rho C_p \mathbf{V} \cdot \nabla_h T \, dz = -\int_{z_0}^{0} \rho C_p \left(u \frac{\partial T}{\partial x} + v \frac{\partial T}{\partial y} \right) dz,$$

where ρ is the density of seawater; C_p is the specific heat capacity of seawater at constant pressure; $\mathbf{V}$ is the horizontal velocity vector, which is $u\mathbf{i} + v\mathbf{j}$ with u and v their components in the zonal and meridional direction, respectively; and ∇_h is horizontal gradient vector, defined as $\partial/\partial x\mathbf{i} + \partial/\partial y\mathbf{j}$. Horizontal heat advection in the upper 50 m from 19 IPCC AR4 coupled GCMs is calculated for the period January 1980–December 1999 and is compared with that from SODA.

The spatial distribution of the biases in horizontal heat advection relative to SODA is shown in Fig. 7. Cold advection is found in most of the stratus region in SODA (top-left panel in Fig. 7). In many models, positive (warm) biases of horizontal heat advection are evident in most of the region, suggesting that these biases largely contribute to the warm SST biases in most models. However, positive biases are not dominant in some models such

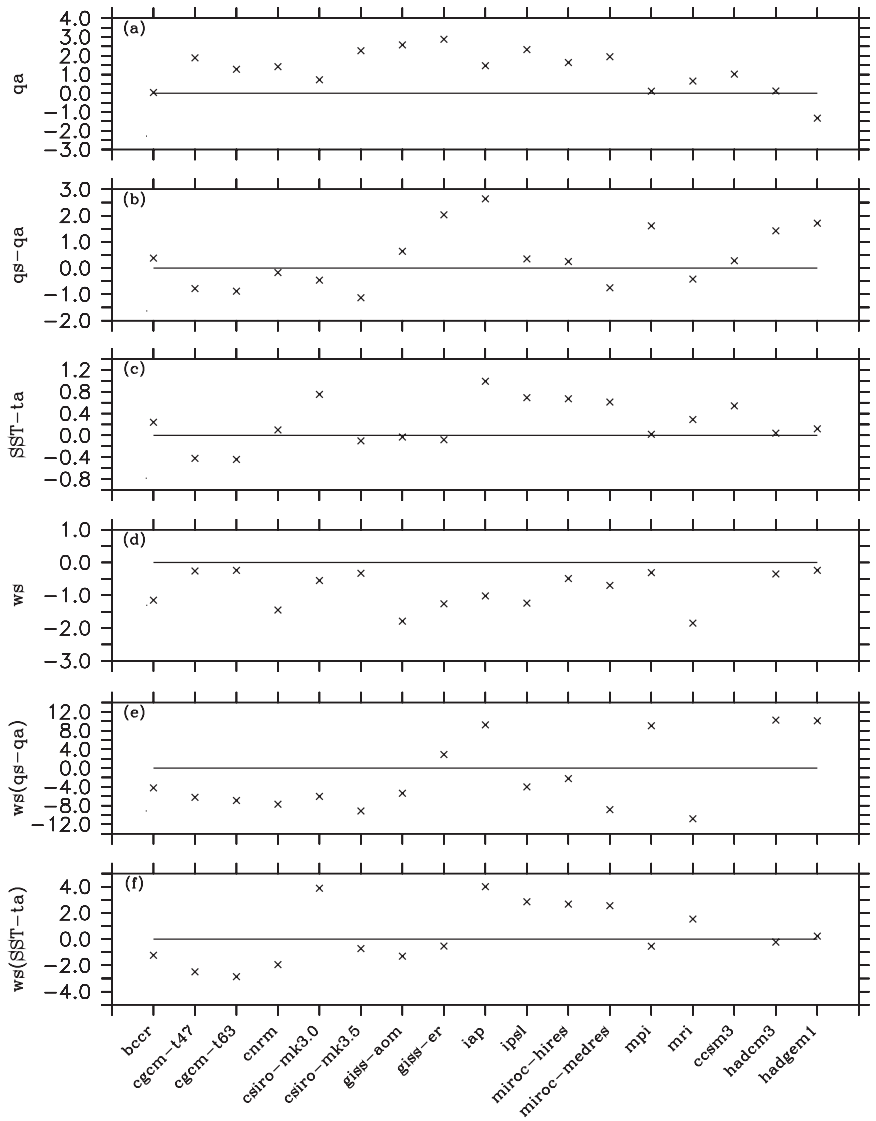

FIG. 5. Biases of (a) surface air specific humidity at 2 m (qa, g kg^{-1}), (b) difference between the saturation and air specific humidity (qs, g kg^{-1}), (c) difference between SST and air temperature at 2 m (SST − T_a, °C), (d) wind speed (m s^{-1}) at 10 m, (e) ws (qs − qa) (m s^{-1} g kg^{-1}), and (f) ws (SST − T_a) (m s^{-1} °C) in 17 IPCC AR4 coupled GCMs area averaged in 20°–5°S, 100°–70°W. Biases are computed relative to atmospheric and oceanic variables from the OAFlux monthly estimates during July 1983–December 1999; horizontal lines denote zero biases.

as BCCR, CNRM, INGV, and MPI. The area-average biases in each model are shown in Fig. 8. While zonal currents (u) in most models are weaker relative to that (-4.6 cm s^{-1}) in SODA, meridional currents (v) in most models are slightly greater than that (-1.6 cm s^{-1}) in SODA. However, the zonal gradient of temperature ($-dT/dx$) is underestimated relative to 0.233 K (100 km)$^{-1}$, and the meridional gradient of temperature ($-dT/dy$) is overestimated relative to SODA [-0.035 K (100 km)$^{-1}$]. Thus, the zonal cold heat advection in most models is underestimated relative to SODA (-17 W m^{-2}), and the meridional warm heat advection in models can be weaker or stronger than that (9 W m^{-2}) in SODA, with smaller errors than the zonal cold heat advection. Therefore, the errors in zonal cold advection appear to be the primarily source of warm SST biases in this region in most models.

2) RELATIVE ROLES OF GEOSTROPHIC AND EKMAN HEAT TRANSPORTS

Zheng et al. (2010) examined heat transport due to both Ekman and geostrophic currents in OGCM experiments

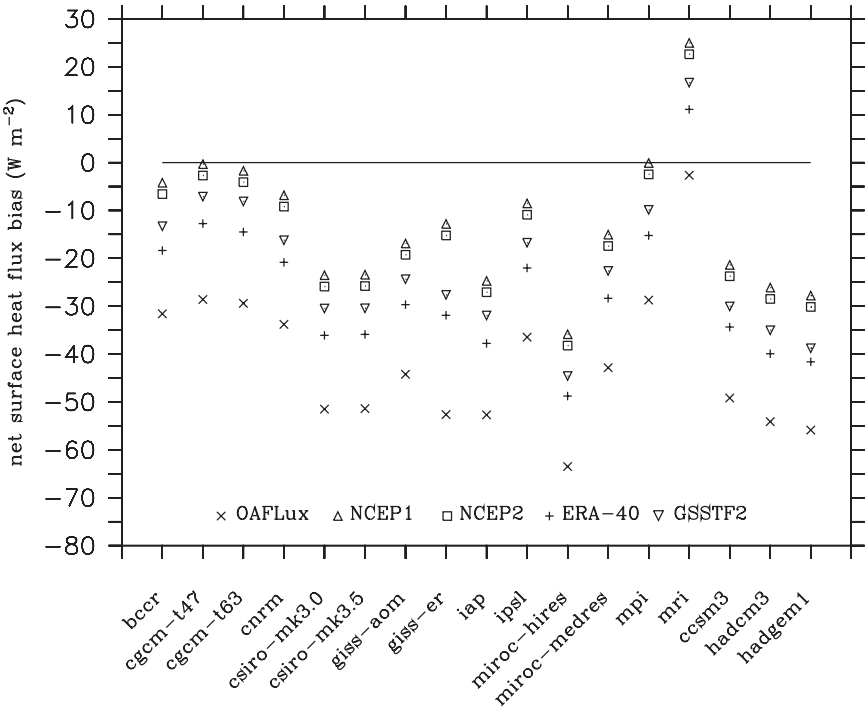

FIG. 6. Biases of net surface heat flux (W m^{-2}) in 17 IPCC AR4 coupled GCMs area averaged in 20°S–5°S, 100°–70°W relative to OAFlux (×), NCEP-1 (△), NCEP-2 (□), ERA-40 (+), and GSSTF2 (▽) for the period January 1988–December 1999. Horizontal lines denote zero biases.

and demonstrated that both of them significantly contribute to the upper-ocean heat budget in the SEP region and that the spatial distribution of these components are notably different. Following the analysis of Zheng et al., Ekman and geostrophic heat advection in the upper 50 m are computed using the output of IPCC CGCMs. Geostrophic velocities are derived from the model temperature and salinity. Ekman currents are computed as the difference between the total velocity and the geostrophic velocity (a residual from the total). It is demonstrated that Ekman currents calculated as a residual are a good approximation based on the comparison of those calculated from SODA with Ekman transports directly calculated from wind stresses (Zheng et al.). Since the ocean processes and the resulting impacts on SST biases near the coast and in the open ocean in the southeast Pacific Ocean are quite different, it is necessary to examine the upper-ocean processes in the open ocean and coastal region separately. In this study, the coastal region is defined as the area where strong observed Ekman heat advection and coastal upwelling generally occur (within 5° of the coastline). The open ocean is defined as the rest of the analysis area (20°–5°S, 100°–70°W).

Figure 9 shows the spatial distribution of the biases in geostrophic heat advection relative to that from SODA (top left panel) over the period January 198 –December 1999. In SODA, cold advection is evident in the open ocean and warm advection is found in the vicinity of the coastal region. Positive biases of geostrophic heat advection are dominant in the open ocean in most models. Some models do not have sufficient resolution to generate the very narrow warm advection near the coast, which is evident in SODA.

Figure 10 shows the spatial distribution of the biases of Ekman heat advection in the upper 50 m from models relative to that in SODA (top left panel) over the period January 1980–December 1999. In SODA, Ekman currents cause warming in the open ocean and cooling near the coast. Positive biases in Ekman heat advection are dominant in the open ocean in most models except BCCR, CNRM, INGV, MPI, MRI, and PCM. Similar to patterns of geostrophic heat advection, some models do not resolve the large cooling near the coast, which is evident in SODA.

Spatial distributions of geostrophic and Ekman heat advection from SODA (Figs. 9 and 10) indicate that the sign of these terms near the coast is opposite that in the open ocean. Thus, processes that are responsible for the warm SST biases in the open ocean and near the coast are likely to be different. To identify the different

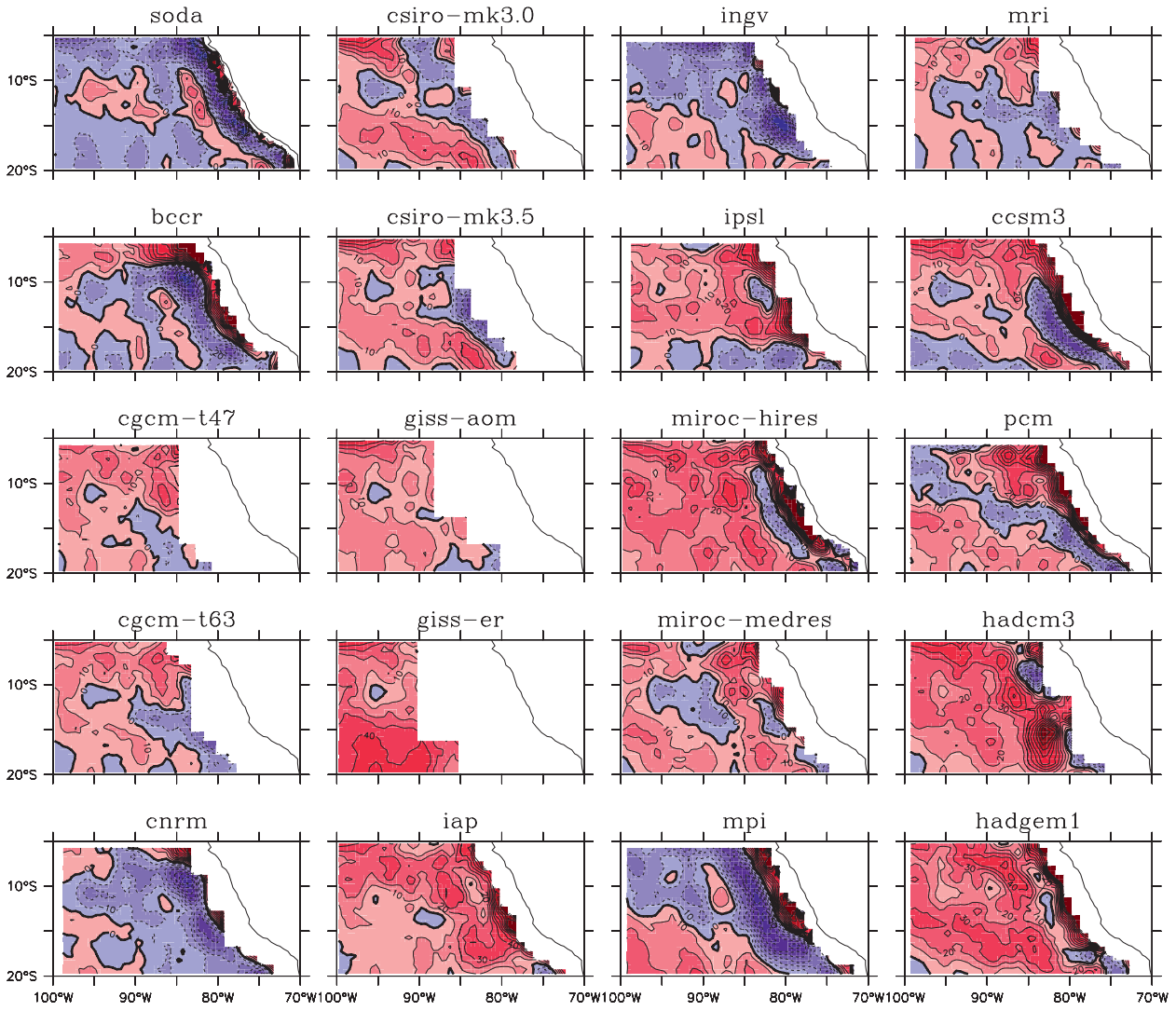

FIG. 7. Spatial distribution of the biases in horizontal heat advection (shading contours; W m^{-2}) in the upper 50 m from 19 IPCC AR4 coupled GCMs. The bias of model horizontal heat advection is relative to that from SODA over the period January 1980–December 1999. (top left) Horizontal heat advection in the upper 50 m.

processes in these regions, further analyses are performed separately for the coastal region and the open ocean.

Figure 11 shows the biases in geostrophic and Ekman velocities and heat advection in CGCMs averaged over the entire area of the analysis (20°–5°S, 100°–70°W), the coastal region, and the open ocean. These biases are computed relative to the averages of these quantities from SODA, shown in Table 3. In SODA, geostrophic currents cause warming (cooling) in the coastal (open ocean) region. In contrast, Ekman currents cause cooling (warming) in the coastal (open ocean) region. The time-mean cooling (−38 W m^{-2}) in the coastal region from Ekman currents is much larger than the time-mean warming (14 W m^{-2}) from geostrophic currents. In most models, the magnitude of biases in the area-averaged Ekman heat advection is much larger than that of geostrophic heat advection for both the coastal region and open ocean. The area-average Ekman heat advection has relatively large positive biases (warming the ocean), both in the coastal region (ranging from 20 to 80 W m^{-2}) and open ocean (ranging from 5 to 25 W m^{-2}). Small positive biases (from 0 to 10 W m^{-2}) in geostrophic heat advection are found in the open ocean for most models, while negative biases from about −20 to −30 W m^{-2} are found in the coastal region.

To further examine how these biases are generated, geostrophic and Ekman currents and temperature from each model are described in Figs. 12 and 13, respectively. In the open ocean, northwestward geostrophic

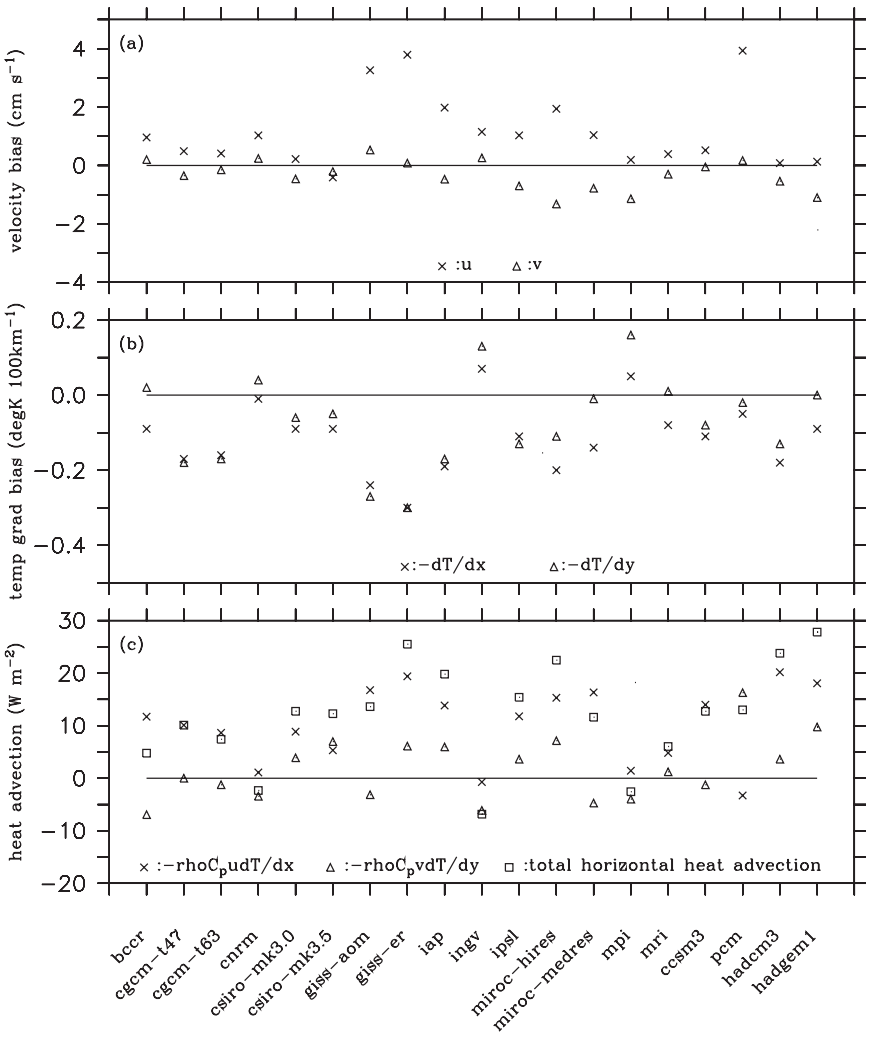

FIG. 8. Biases of (a) velocity (u, v: cm s^{-1}), (b) horizontal temperature gradient [$-dT/dx$, $-dT/dy$: K (100 km)$^{-1}$], and (c) horizontal heat advection and its zonal and meridional components (W m^{-2}) in the upper 50 m from 19 IPCC AR4 coupled GCMs averaged in 20°–5°S, 100°–70°W. Biases are computed relative to those from SODA during the period January 1980–December 1999; "×" denotes the biases of variables in the zonal direction (u, dT/dx, $-\rho C_p u dT/dx$), "Δ" denotes the biases of variables in the meridional direction (v, $-dT/dy$, $-\rho C_p\, v dT/dy$), and "1" denotes the biases of total horizontal heat advection. Horizontal lines denote zero biases.

currents generally bring cold water near the coast to the open ocean (top left panel in Fig. 12). Most models generate a similar distribution of geostrophic currents and temperature, and the biases in currents are small (Fig. 11c), resulting in relatively small positive biases of geostrophic heat advection in the open ocean. In the coastal region, geostrophic currents are overestimated in most models but negative biases in heat advection are evident (Fig. 11b) because most models do not resolve large warming due to geostrophic currents right near the coast, which is evident in SODA (Fig. 9).

Southwestward Ekman currents bring warmer water from low to higher latitude (top left panel in Fig. 13), and thus Ekman transport provide warming in most of the area in the open ocean. Since the angles between the direction of Ekman currents and the isotherms in the open ocean are generally smaller than those for geostrophic currents, the magnitude of Ekman heat advection in the upper 50 m is comparable to that of geostrophic heat advection even though the Ekman currents in this layer are much stronger (Table 3). In contrast to the relation between the direction of Ekman currents and isotherms in SODA, the isotherms in models are more zonal in the open ocean and thus the Ekman currents can affect SST warm biases in two ways. Although the Ekman currents tend to bring cold water from the coastal region to the

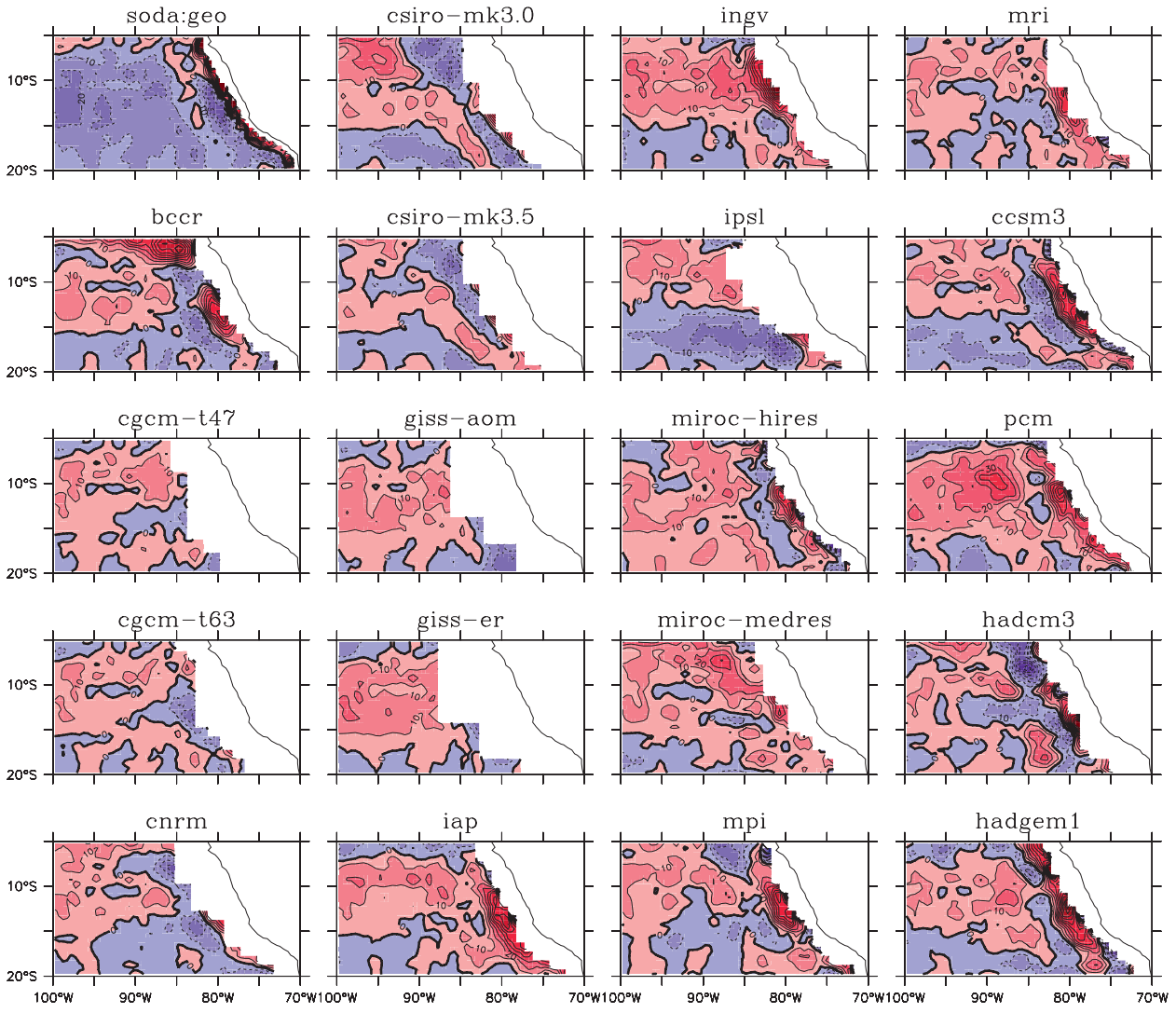

FIG. 9. As in Fig. 7 but for geostrophic heat advection (W m^{-2}).

open ocean less efficiently, they also tend to bring warmer water to higher latitude more efficiently than observed even though those currents are relatively weak in the models (Fig. 11f). Hence, overall positive (warm) biases in Ekman heat advection are generated in the open ocean. These large warm biases in Ekman heat advection along with small warm biases in geostrophic heat advection in the open ocean (Fig. 11c) cause SST warm biases. In the coastal region, Ekman currents cause cooling because they advect cold upwelled water in the offshore direction (top left panel in Fig. 13). Since Ekman currents in the coastal region are underestimated in most models (Fig. 11e) and the large cooling effect of Ekman transport (which is evident in SODA) is not well resolved in most models (Fig. 10), the cooling due to advection is reduced, resulting in positive biases of Ekman heat advection.

3) VERTICAL HEAT ADVECTION AND COASTAL UPWELLING

Figures 14c and 14f show the vertical advection term defined as $-\rho C_p w dT/dz$ (W m^{-2}) in the upper 50 m for the coastal region and the open ocean. While no systematic bias of this term is found in the coastal region, significant cold biases are evident in the open ocean. The errors in downward velocity and the resultant heat advection may be partly responsible for the cold biases in the open ocean. In the coastal region, upwelling is overly weak in most models (Fig. 14d). However, because of the overly large temperature gradient in some models (Fig. 14e), these errors compensate and systematic biases are not found (Fig. 14f). Also, it is not clear whether vertical heat advection in the upper 50 m is directly related to

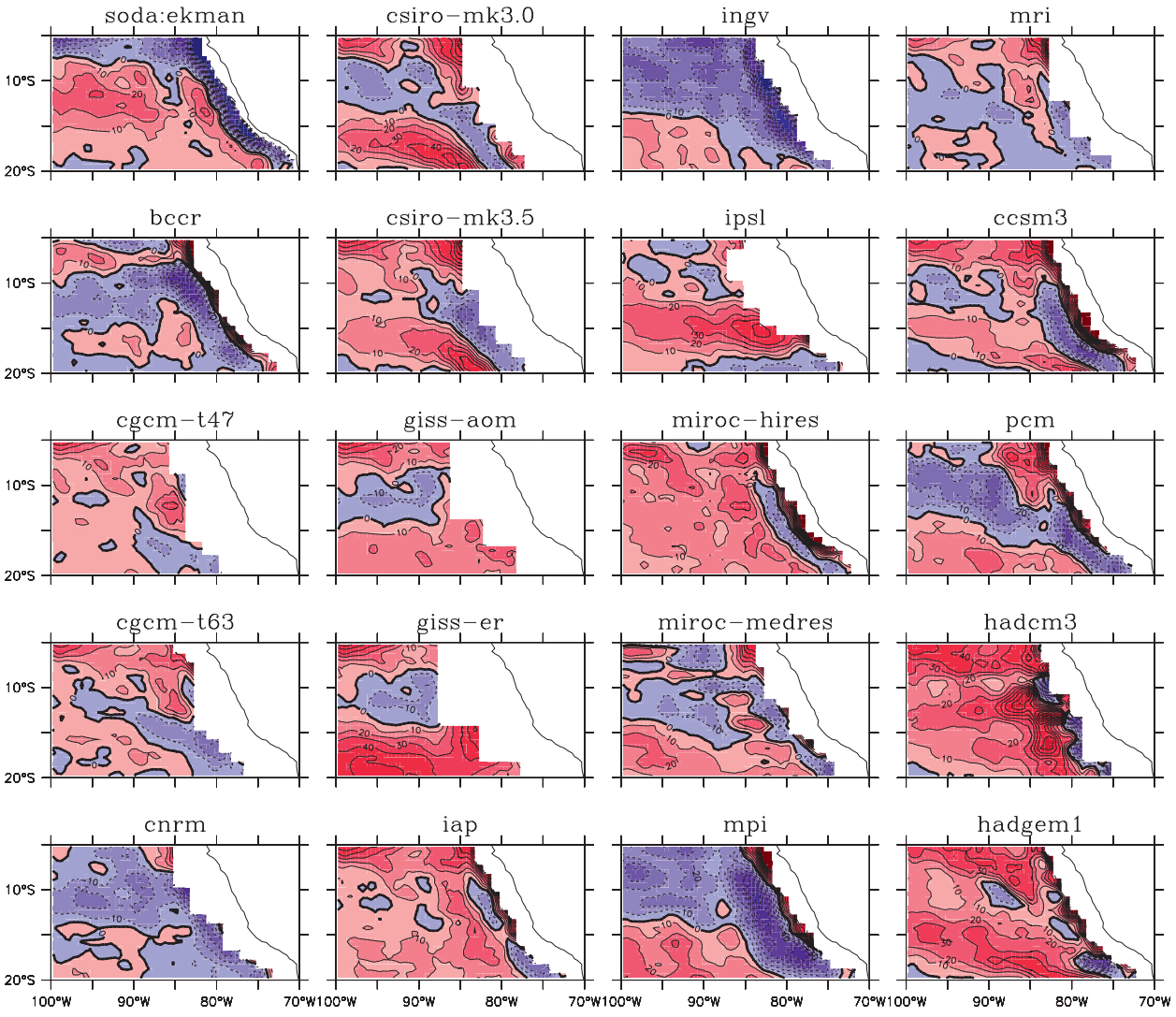

FIG. 10. As in Fig. 7 but for Ekman heat advection (W m^{-2}).

SSTs in the coastal region since the mixed layer depth is generally shallower than 50 m and thus large heat advection around 50 m may not directly influence SSTs.

To further examine the influence of vertical heat advection on SSTs, the circulation and temperature in the zonal–vertical plane are described. Figure 15 shows the zonal circulation and temperature along 15°S averaged over January 1980–December 1999 from SODA and CGCMs. Strong coastal upwelling occurs within 3°–5° offshore in SODA. This cold upwelled water is then transported away from the coast by the mean currents. The coastal upwelling is underestimated in most models, and temperature profiles near the coast suggest that cold subsurface water affects SSTs less than those in SODA. This is further demonstrated in the depth of the 18°C isotherm along 15°S (Fig. 16). While 18°C isotherms are shallower in most models than those in SODA west of 78°W, the upwelling is not strong enough to bring water colder than 18°C to the surface at the coast. The upwelling zone is broader than in SODA in most models, which can also influence SST in the open ocean through the vertical heat advection term, but, overall, the magnitude is much smaller than horizontal heat advection (Figs. 11 and 14). Similar results are found at other latitudes between 10° and 20°S.

The too broad and weak upwelling could be due to a combination of the coarse horizontal resolution of ocean models (Table 1) and underestimates of alongshore winds. Figure 17 shows the strength of alongshore wind stress in CGCMs compared to that in SODA. All models have weaker alongshore wind stresses at most latitudes. Hence, the relation between biases in upwelling and alongshore winds is consistent. However, it is difficult to identify the

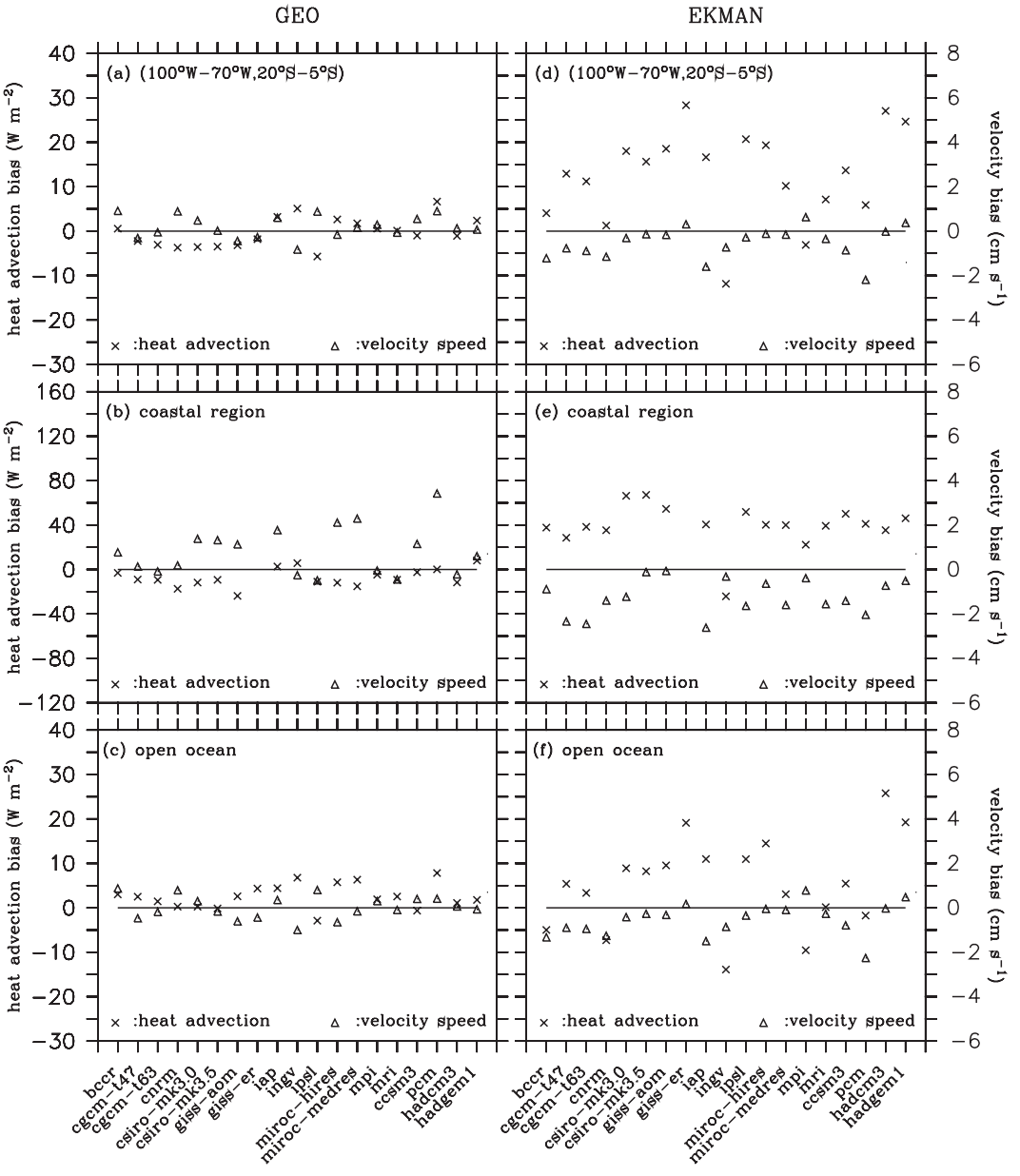

FIG. 11. Biases of geostrophic heat advection (denoted by "×"; W m^{-2}) and biases of geostrophic current speed (denoted by "△"; cm s^{-1}) averaged over (a) 20°–5°S, 100°–70°W, (b) the coastal region between 20° and 5°S, and (c) the open ocean in the upper 50 m from 19 IPCC AR4 coupled GCMs. (d)–(f) As in (a)–(c) but for biases of Ekman heat advection and current speed. Biases of these variables are relative to those from SODA during January 1980–December 1999; the ordinate on the left (right) side of the panel indicates biases in heat advection (velocity). Coastal region is defined as the area 5° from the coastline. Horizontal lines denote zero biases.

ultimate sources of these biases as a variety of processes in the atmosphere and ocean as well as air–sea feedback are involved in determining them in CGCMs.

5. Discussion

This study focuses on identifying the errors of upper-ocean processes and air–sea fluxes in CGCMs that could contribute to SST biases in the SEP region. It is worth reemphasizing that the net causes of these SST biases are likely ultimately determined by a combination of atmospheric, land, and oceanic processes, along with air–sea feedback processes that could amplify the errors in both AGCM and OGCM components. For example, strong alongshore winds at the coast of Chile and Peru are primarily caused by the great height of the Andes

TABLE 3. Magnitude of geostrophic, Ekman velocity, and the resultant heat advection from SODA averaged in 20°–5°S, 100°–70°W; the coastal region; and the open ocean over the period January 1980–December 1999. Units: centimeters per second for velocity and watts per meter squared for heat advection.

SODA	V_{geo}	V_{Ek}	H_{geo}	H_{Ek}
20°–5°S, 100°–70°W	2.95	4.86	−6	−3
Coastal region	2.28	4.31	14	−38
Open ocean	3.12	5.00	−11	6

Cordillera that acts as a barrier to zonal flow in the South Pacific (Garreaud and Muñoz 2005). In fact, a recent CGCM study (Gent et al. 2009) demonstrated that a high-resolution AGCM that can better resolve the orography of the Andes Cordillera allows strongest surface winds in the upwelling region to be located much closer to the coast, which in turn generate stronger coastal upwelling, resulting in reduced SSTs. The colder SST and near-surface air temperature generate more stratus clouds, which shield the sunlight reaching the ocean and further reduce the SST. Further studies that focus on atmospheric, land, and air–sea feedback processes are necessary to precisely identify the combination of sources of SST biases in CGCMs in this region.

In this study, OAFlux and SODA are primarily used to determine CGCM errors in surface heat fluxes and upper-ocean currents and temperatures. While these datasets are useful for evaluating current CGCMs that include substantial errors in surface fluxes and upper-ocean variables in the SEP region, there could be significant

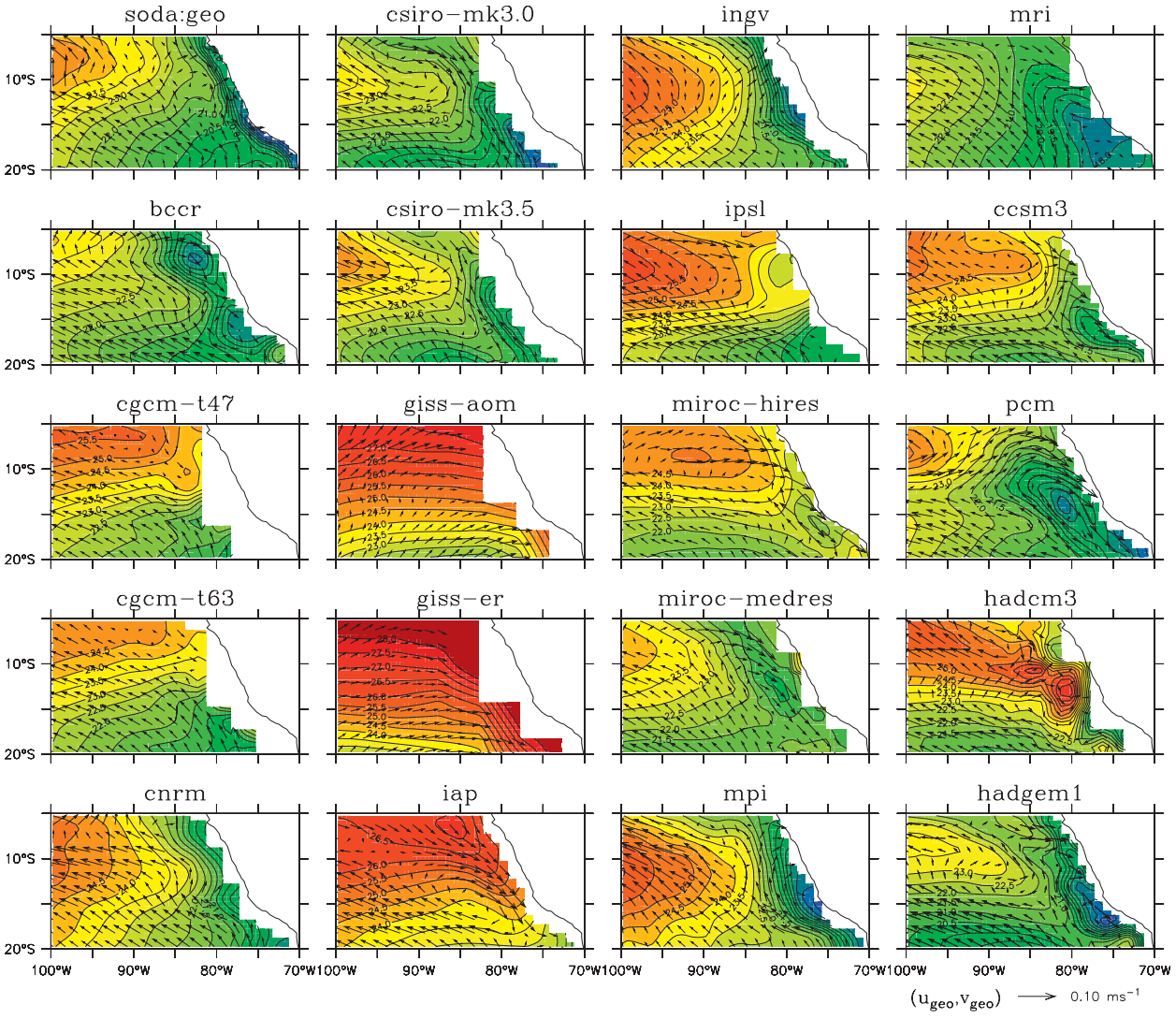

FIG. 12. Geostrophic currents (arrows) and temperature (shading) in the upper 50 m from (top left) SODA and IPCC AR4 CGCMs (other panels).

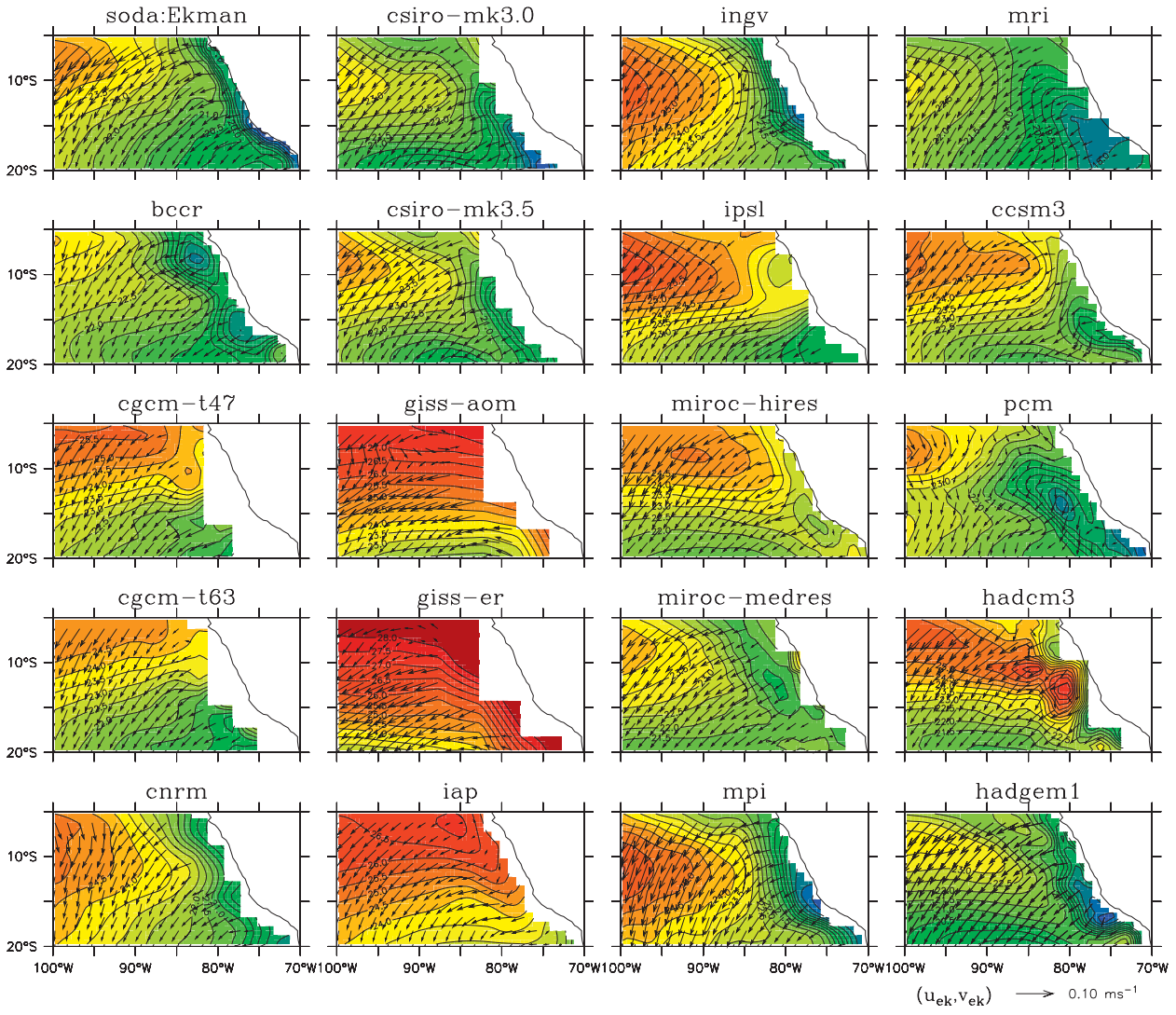

FIG. 13. As in Fig. 12 but for Ekman currents.

uncertainties in these analyses. It has been difficult to validate these datasets since there were few in situ measurements of upper-ocean and surface fluxes in the SEP region until recently. Intensive in situ observations of the upper-ocean and atmospheric boundary layer, including air–sea fluxes, were conducted in fall 2008 as part of VOCALS (Wood et al. 2007). A substantial amount of data collected during the VOCALS REx would be useful to evaluate a variety of surface flux datasets and ocean analysis and to validate various schemes used in the analysis, such as the bulk flux algorithm. Hopefully, these global datasets will be further improved after the validation and evaluation of the analyses based on comparison using the data from VOCALS REx as well as other observations.

Since none of the IPCC AR4 coupled GCMs resolve mesoscale and submesoscale eddies because of their coarse horizontal resolution, the role of eddy activity in the warm SST biases could not be investigated in this study. The precise role of eddies in the heat budget of the SEP is still controversial. For example, recent independent high-resolution modeling studies (Zheng et al. 2010; Toniazzo et al. 2010) indicated that long-term mean area-averaged eddy heat flux divergence is small over the SEP region. Conversely, McWilliams and Colas (2010) and F. Colas et al. (2011, personal communication) examine the heat balance in the Peru–Chile Current System (PCS) using regional ocean models (ROMs), and show that both the total mean-flow advection and eddy heat flux are necessary to sustain the oceanic cooling in the PCS. It should be noted that the domain of their analysis is limited to a region in the PCS (700 km from the coastline), which is much smaller than the scale of

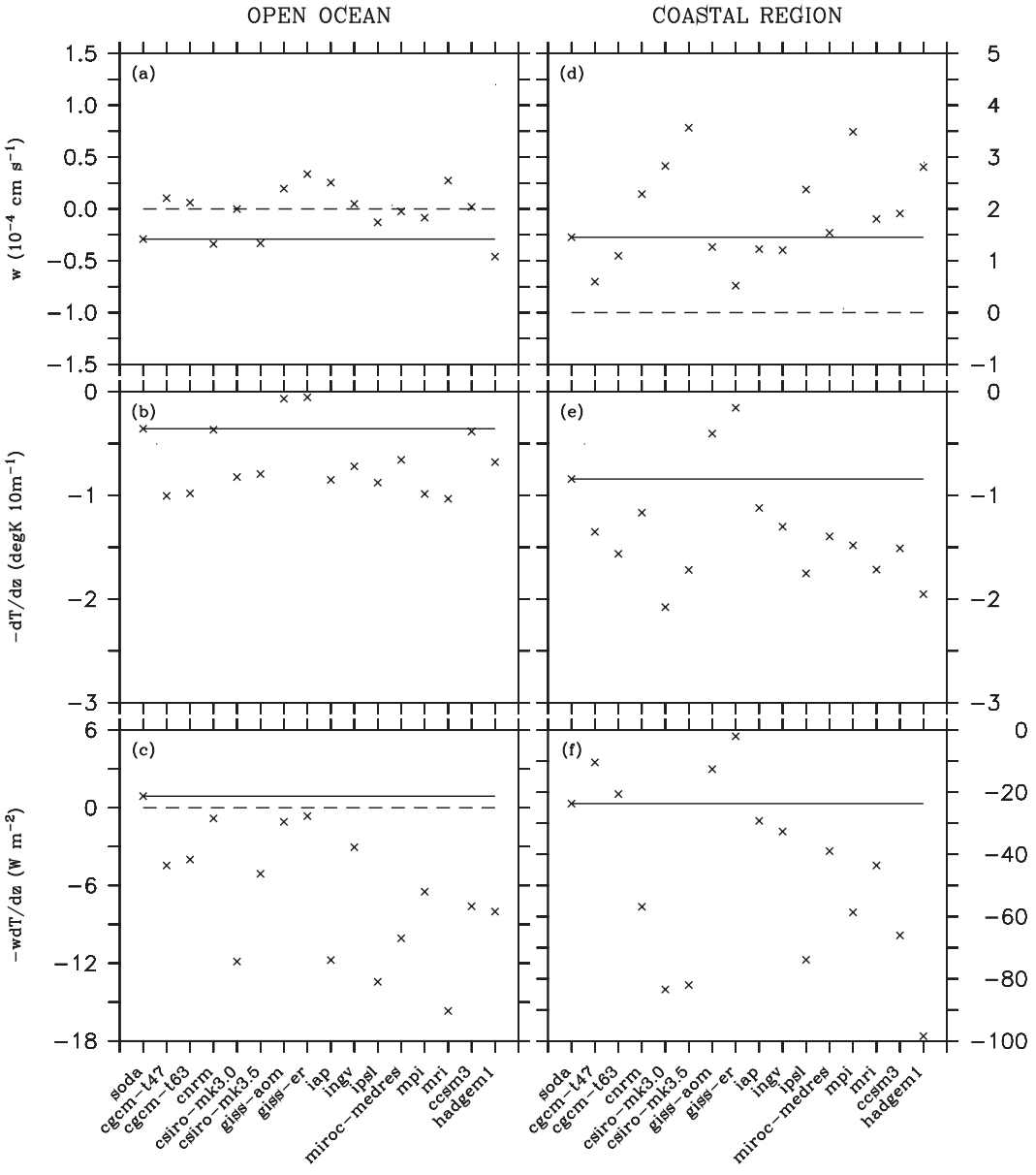

FIG. 14. (a) Vertical velocity (w, 10^{-4} cm s^{-1}) averaged in the upper 50 m, (b) $-dT/dz$ [K (10 m)$^{-1}$] averaged in the upper 50-m depth, and (c) $-\rho C_p wdT/dz$ (W m^{-2}) integrated in the upper 50 m and then averaged in the open-ocean area from SODA and 15 IPCC AR4 coupled GCMs. (d)–(f) As in (a)–(c) but for those averaged in the coastal region. Horizontal solid lines denote zero biases; horizontal dashed lines denote zero values.

the stratus cloud deck and warm SST biases in the SEP. This result is consistent with our previous study that shows the importance of eddy heat flux near the coast (Fig. 12 in Zheng et al. 2010).

More recent studies suggest that eddies can contribute to lowering the upper ocean's heat content (and hence SST) by bringing a cold, fresh Pacific intermediate layer closer to the surface. Vertical mixing associated with double diffusion between the eastern South Pacific Intermediate Water and the surface layer appears to play an essential role in maintaining the upper ocean's heat content and salt balance based on the analysis of VOCAL REx data (e.g., Straneo et al. 2010; Zappa et al. 2010). Despite the controversies about the role of eddies in the maintenance of cold waters in the SEP, all recent studies described above affirm the leading importance of heat advection in controlling SSTs in this region. Since it is likely that horizontal and vertical heat advection significantly contribute to maintaining cold SSTs—at least for the scale of the stratus cloud deck in the SEP—the evaluation of

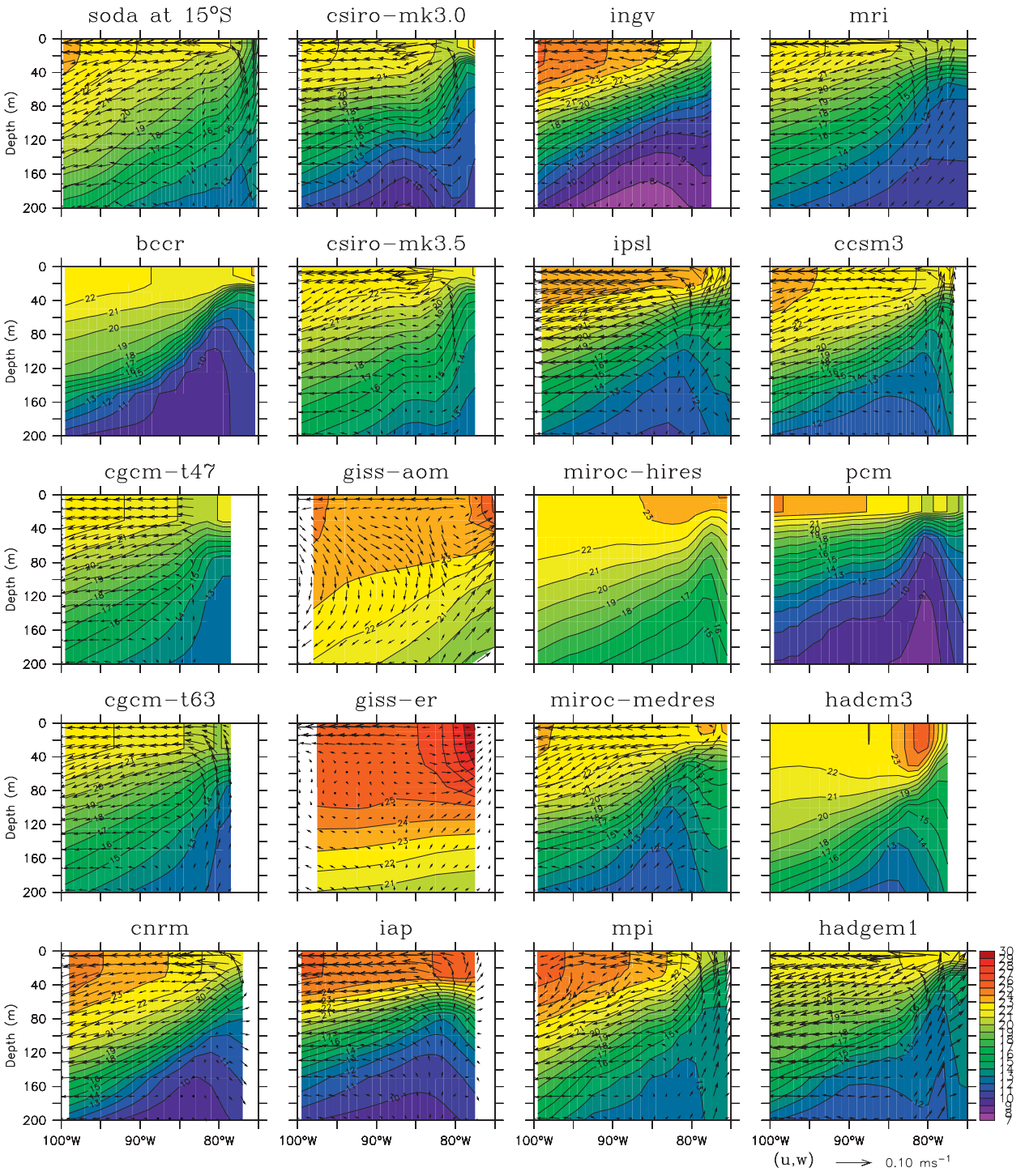

FIG. 15. Circulation (vectors, m s^{-1}) and temperatures (shading contours; °C) in the zonal–vertical plane at 15°S averaged over January 1980–December 1999 from (top left) SODA and 19 IPCC AR4 coupled GCMs, Contour interval: 1°C.

advection and heat flux terms in models is essential for understanding the cause of the warm SST biases.

An analysis of the upper ocean shows that most CGCMs underestimate coastal upwelling owing to coarse ocean model resolution, so improving the ocean model resolution may help reduce the SST biases by better resolving coastal upwelling. While the alongshore winds in the AGCMs are weaker than observed and partially

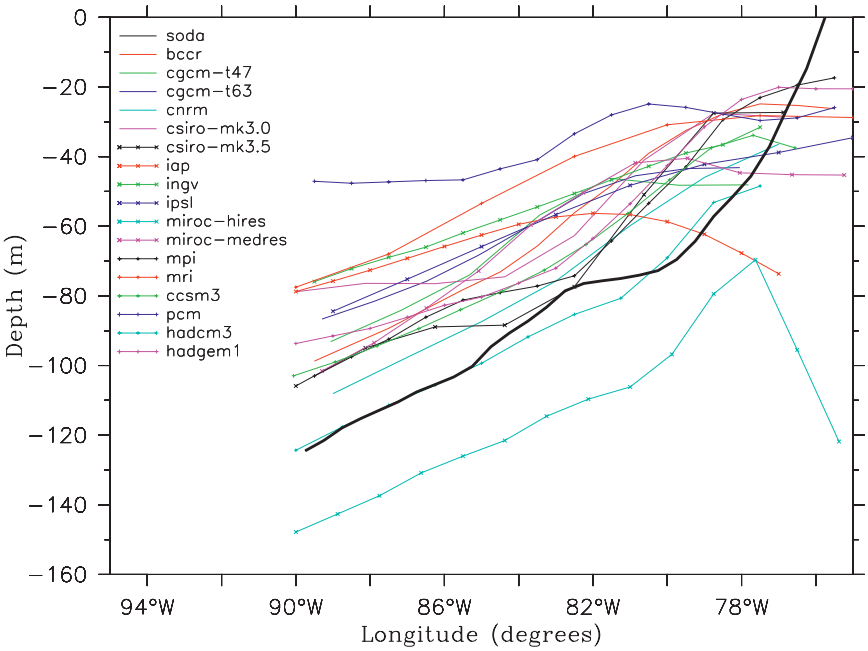

FIG. 16. Depth of the 18°C isotherm along 15°S averaged over the period January 1980–December 1999 from SODA and 17 IPCC AR4 coupled GCMs. Two models (GISS-AOM and GISS-ER) are excluded because of their extreme values (see also Fig. 15).

responsible for the weaker upwelling, the horizontal resolution in the OGCMs is not adequate to resolve strong and narrow upwelling. Accordingly, improving the horizontal resolution in the OGCM component may reduce warm SST biases in the coastal region. Also, if more cold water is upwelled at the coast, warm SST biases in the open ocean would also be reduced by horizontal advection of this water away from the coast.

The result also shows that cold water (less than 18°C) is upwelled to around 30–40-m depth in many models (Figs. 15 and 16), but this does not significantly affect SST, possibly because mixing in the upper layer (i.e., above 40 m) is not sufficiently strong. The improvement of mixing schemes is a major challenge in ocean modeling, but this is a worthwhile endeavor and is likely to also reduce SST biases. For example, OGCM and one-dimensional ocean model experiments could be performed to examine the sensitivity of the upper-ocean temperature and SST near the coast to different mixing schemes. Comparisons with high quality and fine resolution data in the upper ocean obtained during VOCALS REx would be very useful for such studies.

The underestimated alongshore winds in the AGCM component of IPCC AR4 models could be partly attributed to overestimated precipitation in the SEP region (M. Davis et al. 2011, personal communication). Although deep convection is rarely observed in the SEP, many IPCC AR4 models produce substantial precipitation in this region, which is in turn tied to the double intertropical convergence zone (ITCZ) problem (Mechoso et al. 1995; Lin 2007; de Szoeke and Xie 2008). Excess precipitation lowers the sea level pressure because the release of latent heat due to unrealistically high precipitation heats the atmosphere locally. Thus, the subtropical high is weakened, leading to weaker alongshore winds. Lin (2007) hypothesized that the overestimation of tropical precipitation in IPCC AR4 models is caused by their lack of the observed self-suppression processes in tropical convection, such as the sensitivity of convective updrafts to lower tropospheric moisture, the cooling and drying of the boundary layer by convective downdrafts, and the warming and drying of the lower troposphere by mesoscale downdrafts. Including these processes in model deep-convection schemes may help lead to a more realistic upper-ocean state by reducing the excessive precipitation in the SEP region and enhancing the subtropical high and alongshore winds.

6. Summary

This study investigates processes in the upper ocean and air–sea fluxes that could contribute to systematic SST biases under stratus cloud decks in the southeast Pacific in 19 IPCC AR4 coupled GCMs. Surface fluxes and upper-ocean variables from the output of CGCMs are analyzed and compared with surface flux estimates

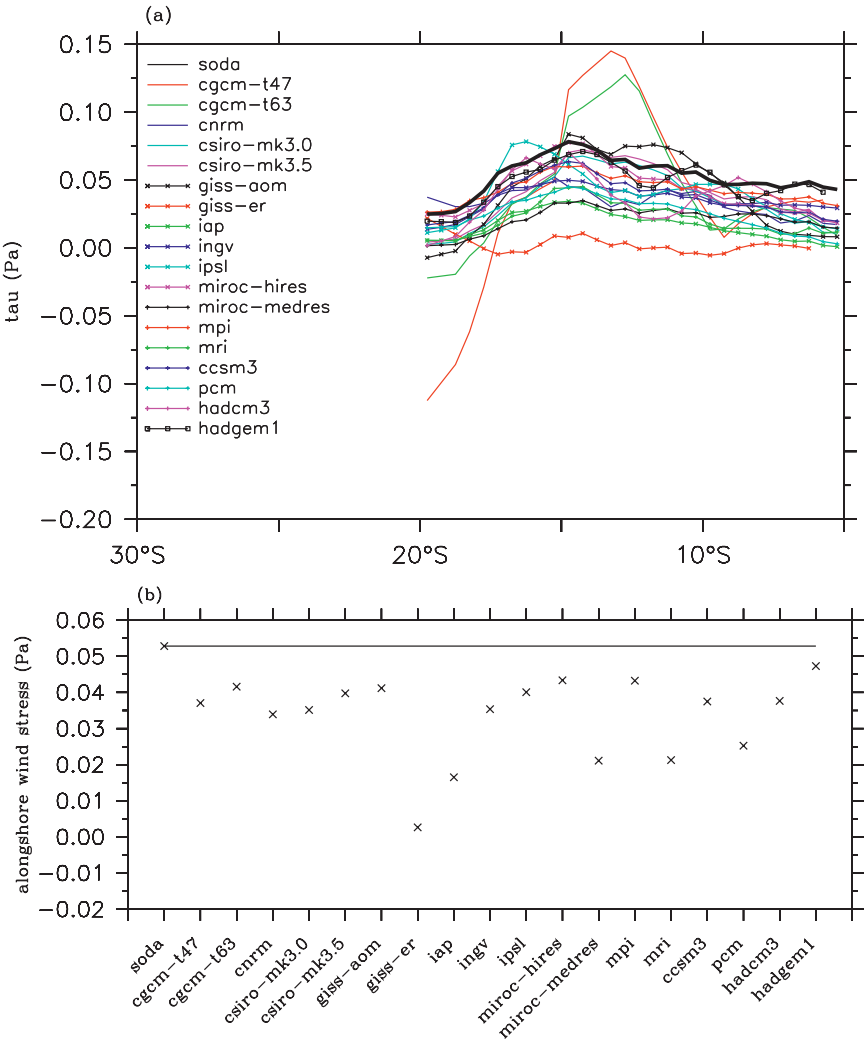

FIG. 17. (a) Alongshore wind stress (Pa) as a function of latitude and (b) alongshore wind stress averaged between 20° and 5°S over the period January 1980–December 1999 from SODA and 18 IPCC AR4 coupled GCMs. The horizontal line in (b) denotes zero biases.

(OAFlux) and the ocean analysis (SODA) derived from a variety of satellite measurements and reanalyses. Nearly universal warm SST biases in CGCMs are found, and the biases are larger in the northern part of the stratus region, especially north of 20°S.

In contrast to warm SST biases, negative biases (cooling the ocean) in net surface heat flux are found in most CGCMs, indicating that errors in surface heat fluxes do not significantly contribute to their SST biases but, in fact, damp warm SST biases. The negative biases in latent heat flux and longwave radiation are mostly responsible for the negative net surface heat flux biases. Positive biases in shortwave radiation are found in most models because they do not generate sufficient stratus clouds.

Since horizontal heat advection strongly influences the annual mean heat budget, and thus SST (Colbo and Weller 2007; Zheng et al. 2010), heat advection due to geostrophic and Ekman currents is estimated using the CGCM outputs. Our results suggest that positive biases of Ekman heat advection primarily contribute to the warm SST biases, while the contribution of the errors in geostrophic heat advection is also significant. Near the coast of Peru and Chile, warm SST biases are attributed to weaker Ekman currents that transport less cold upwelled water from the coast offshore. In the open ocean, southwestward Ekman currents bring warm water near the equator southward more efficiently because the isotherms in CGCMs are more zonal than in observations. Most CGCMs underestimate alongshore winds and coastal upwelling, which contributes to the warm SST biases both in the offshore and coastal regions. Upwelling in most CGCMs is weaker and broader than

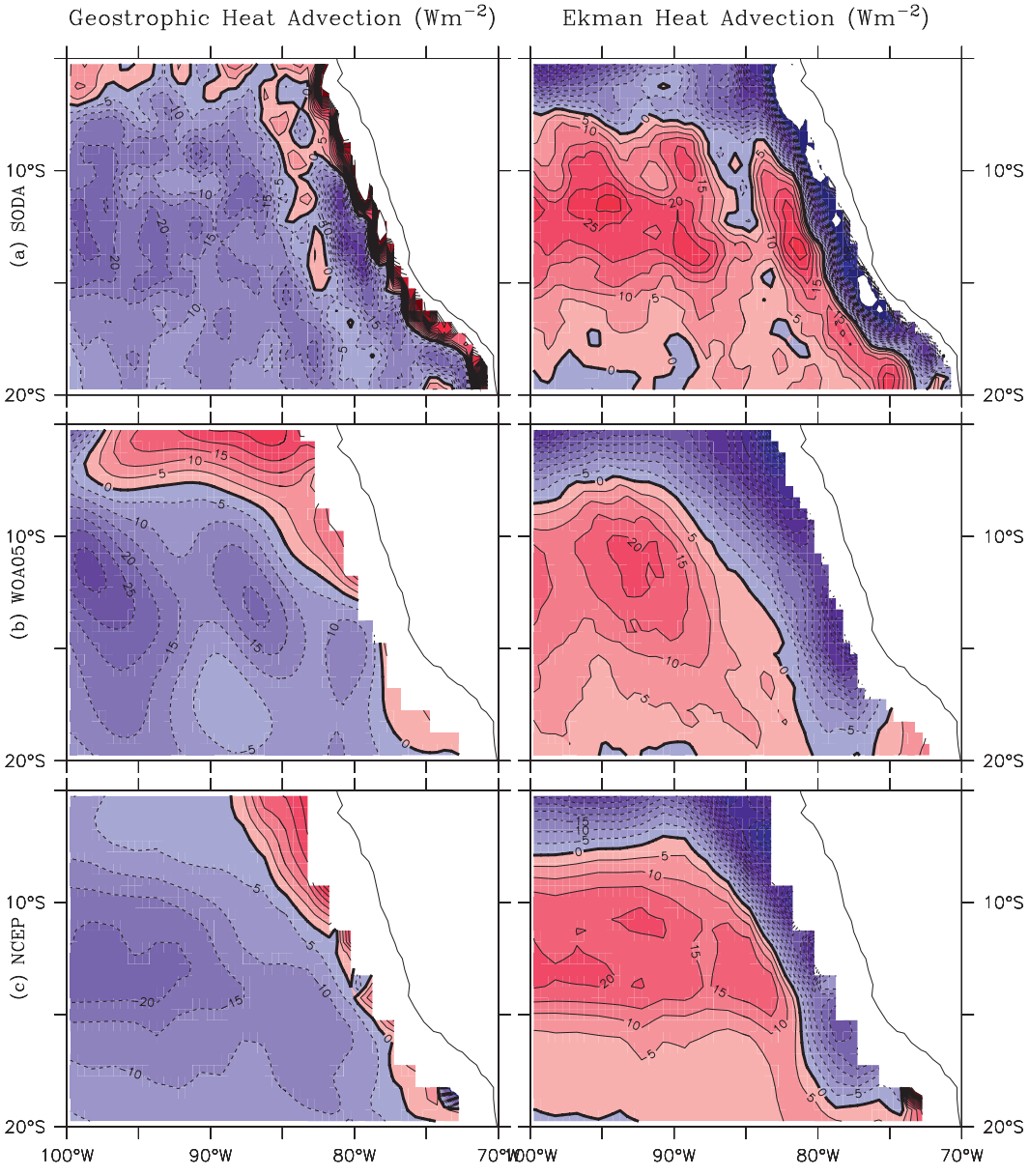

FIG. A1. Comparisons of the spatial distribution of annual mean geostrophic and Ekman heat advection integrated in the upper 50 m of the southeast Pacific Ocean between SODA and *WOA05* as well as NCEP Pacific Ocean analysis.

observations. It is suggested that the coarse resolution of the OGCM component is partially responsible for the underestimated upwelling in CGCMs. Therefore, we hypothesize here that the improvement of horizontal resolution in the OGCM components of CGCMs will reduce the warm SST biases in the SEP region. Improvement in resolution and in convection schemes in the AGCM component of CGCMs could also help better simulate alongshore winds, thus leading to a more realistic upper-ocean state.

Acknowledgments. We are greatly indebted to all those who contributed to the observations and global datasets used in this study. We thank Simon de Szoeke, Editor Robert Wood, and two anonymous reviewers for their helpful comments. Computational facilities have been provided by the National Oceanic and Atmospheric Administration (NOAA). Yangxing Zheng is supported by NSF Grant OCE-0453046. Toshiaki Shinoda is supported by NOAA CPO Grant GC-10-400 under the Modeling, Analysis, and Prediction (MAP) Program; the

NSF Grants OCE-0453046, AGS-0966844, and ATM-0745897; and 6.1 projects sponsored by the Office of Naval Research (ONR) under Program Element 601153N. Jia-Lin Lin is supported by the National Aeronautics and Space Administration (NASA) under the MAP program and by NSF Grant ATM-0745872.

APPENDIX

Comparison of SODA Ocean Analysis with *WOA05* and NCEP Pacific Ocean Analysis

The SODA analysis is compared with monthly climatology data from *WOA05* and NCEP Pacific Ocean analysis. Figure A1 shows the spatial distribution of annual mean geostrophic and Ekman heat advection integrated in the upper 50 m of the southeast Pacific Ocean. The period for the averaging in SODA and NCEP is January 1980–December 1999. *WOA05* uses monthly climatology temperature and salinity datasets. Geostrophic heat advection is computed from geostrophic currents derived from temperature and salinity profiles. To compare SODA with *WOA05*, the Ekman heat advection in *WOA05* is computed using ERA-40 monthly climatology wind stress (since SODA utilizes ERA-40 wind stress) and the temperatures from *WOA05*. Ekman heat advection in SODA and NCEP is computed as the difference between total heat advection and geostrophic heat advection. It should be noted that Ekman heat advection computed by the two methods is similar in SODA (Zheng et al. 2010). There is good agreement in the spatial distribution of annual-mean horizontal heat advection. One advantage of using SODA instead of other datasets is the relatively fine resolution near the coastal region, which can better resolve coastal processes.

We further compute the area-averaged values in the total coastal region and open ocean (same definition as in the paper), listed in Table A1. The area-averaged values are important as they are used to measure the model biases in this study. The consistency in area-averaged horizontal heat advection among different datasets indicates that SODA can be used for evaluating ocean heat advection in IPCC models. Clearly, the difference in heat advection near the coastal region can be affected by the difference in resolution near the coast in SODA and other datasets. For example, large cooling by Ekman heat advection adjacent to the coastline in *WOA05* and NCEP vanish owing to coarse resolution, thus leading to weak cooling. Based on our analysis, warm SST biases are largely attributed to positive biases of Ekman heat advection in IPCC models relative to SODA. If we use *WOA05* data and NCEP Pacific Ocean analysis, this conclusion is not changed since the discrepancies in these values are not sufficiently large to affect the sign of biases for most models. For example, Ekman heat advection in *WOA05* and NCEP is 5.6 and 12 W m^{-2} larger than SODA near the coastal region, respectively (Table A1). These numbers are much smaller than warm biases of Ekman heat advection (about 40 W m^{-2}) in most IPCC models shown in Fig. 11e. In the open ocean, the warming induced by Ekman heat advection in *WOA05* and NCEP is only slightly larger than the counterpart in SODA.

TABLE A1. Comparisons of SODA with *WOA05* and NCEP Pacific Ocean analysis in annual mean horizontal area-averaged heat advection of upper 50 m of the SEP. Definitions of coastal and open-ocean values are the same. (Unit: W m^{-2})

	Heat advection	
	Geostrophic	Ekman
	20°–5°S, 100°–70°W	
SODA	−6.0	−2.2
WOA05	−6.7	−3.7
NCEP	−8.2	0.36
	Coastal region	
SODA	14.0	−38.4
WOA05	5.6	−32.8
NCEP	2.3	−26.4
	Open ocean	
SODA	−11.2	6.0
WOA05	−8.5	1.6
NCEP	−10.0	4.2

REFERENCES

Antonov, J. I., R. A. Locarnini, T. P. Boyer, A. V. Mishonov, and H. E. Garcia, 2006: *Salinity*. Vol. 2, *World Ocean Atlas 2005,* NOAA Atlas NESDIS 62, 182 pp.

Bingham, F. M., S. D. Howden, and C. J. Koblinsky, 2002: Sea surface salinity measurements in the historical database. *J. Geophys. Res.,* **107,** 8019, doi:10.1029/2000JC000767.

Boyer, T. P., C. Stephens, J. I. Antonov, M. E. Conkright, L. A. Locarnini, T. D. O'Brien, and H. E. Garcia, 2002: *Salinity*. Vol. 2, *World Ocean Atlas 2001,* NOAA Atlas NESDIS 49, 165 pp.

Brunke, M. A., C. W. Fairall, X. Zeng, L. Eymard, and J. A. Curry, 2003: Which bulk aerodynamic algorithms are least problematic in computing ocean surface turbulent fluxes? *J. Climate,* **16,** 619–635.

Carton, J. A., and B. S. Giese, 2008: A reanalysis of ocean climate using Simple Ocean Data Assimilation (SODA). *Mon. Wea. Rev.,* **136,** 2999–3017.

——, G. A. Chepurin, X. Cao, and B. S. Giese, 2000a: A Simple Ocean Data Assimilation analysis of the global upper ocean 1950–95. Part I: Methodology. *J. Phys. Oceanogr.,* **30,** 294–309.

——, ——, and ——, 2000b: A Simple Ocean Data Assimilation analysis of the global upper ocean 1950–95. Part II: Results. *J. Phys. Oceanogr.,* **30,** 311–326.

Chou, S.-H., E. Nelkin, J. Ardizzone, R. M. Atlas, and C.-L. Shie, 2003: Surface turbulent heat and momentum fluxes over global oceans based on the Goddard satellite retrievals, version 2 (GSSTF2). *J. Climate,* **16,** 3256–3273.

——, ——, ——, and ——, 2004: A comparison of latent heat fluxes over global oceans for four flux products. *J. Climate,* **17,** 3973–3989.

Colbo, K., and R. Weller, 2007: The variability and heat budget of the upper ocean under the Chile-Peru stratus. *J. Mar. Res.,* **65,** 607–637.

de Szoeke, S. P., and X.-P. Xie, 2008: The tropical eastern Pacific seasonal cycle: Assessment of errors and mechanisms in IPCC AR4 coupled ocean–atmosphere general circulation models. *J. Climate,* **21,** 2573–2590.

——, C. W. Fairall, D. E. Wolfe, L. Bariteau, and P. Zuidema, 2010: Surface flux observations on the southeastern tropical Pacific Ocean and attribution of SST errors in coupled ocean–atmosphere models. *J. Climate,* **23,** 4152–4174.

Diaz, H., C. Folland, T. Manabe, D. Parker, R. Reynolds, and S. Woodruff, 2002: Workshop on advances in the use of historical marine climate data. *WMO Bull.,* **51,** 377–380.

Fairall, C. W., E. F. Bradley, J. E. Hare, A. A. Grachev, and J. B. Edson, 2003: Bulk parameterization of air–sea fluxes: Updates and verification for the COARE algorithm. *J. Climate,* **16,** 571–591.

Garreaud, R. D., and R. C. Muñoz, 2005: The low-level jet off the west coast of subtropical South America: Structure and variability. *Mon. Wea. Rev.,* **133,** 2246–2261.

Gent, P. R., S. G. Yeager, R. B. Neale, S. Levis, and D. A. Bailey, 2009: Improvements in a half degree atmosphere/land version of the CCSM. *Climate Dyn.,* **34,** 819–833, doi:10.1007/s00382-009-0614-8.

Gordon, C. T., A. Rosati, and R. Gudgel, 2000: Tropical sensitivity of a coupled model to specified ISCCP low clouds. *J. Climate,* **13,** 2239–2260.

Jones, P. W., 1999: First- and second-order conservative remapping schemes for grids in spherical coordinates. *Mon. Wea. Rev.,* **127,** 2204–2210.

Kalnay, E., and Coauthors, 1996: The NCEP/NCAR 40-Year Reanalysis Project. *Bull. Amer. Meteor. Soc.,* **77,** 437–471.

Kanamitsu, M., W. Ebisuzaki, J. Woollen, S.-K. Yang, J. J. Hnilo, M. Fiorino, and G. L. Potter, 2002: NCEP–DOE AMIP-II Reanalysis (R-2). *Bull. Amer. Meteor. Soc.,* **83,** 1631–1643.

Kiehl, J. T., and P. R. Gent, 2004: The Community Climate System Model, version 2. *J. Climate,* **17,** 3666–3682.

Kubota, M., A. Kano, H. Muramatsu, and H. Tomita, 2003: Intercomparison of various surface heat flux fields. *J. Climate,* **16,** 670–678.

Large, W. G., and G. Danabasoglu, 2006: Attribution and impacts of upper-ocean biases in CCSM3. *J. Climate,* **19,** 2325–2346.

——, J. C. McWilliams, and S. C. Doney, 1994: Oceanic vertical mixing: Review and model with a nonlocal boundary layer parameterization. *Rev. Geophys.,* **32,** 363–403.

Lin, J.-L., 2007: The double-ITCZ problem in IPCC AR4 coupled GCMs: Ocean–atmosphere feedback analysis. *J. Climate,* **20,** 4497–4525.

Locarnini, R. A., A. V. Mishonov, J. I. Antonov, T. P. Boyer, and H. E. Garcia, 2006: *Temperature*. Vol. 1, *World Ocean Atlas 2005,* NOAA Atlas NESDIS 61, 182 pp.

Ma, C.-C., C. R. Mechoso, A. W. Robertson, and A. Arakawa, 1996: Peruvian stratus clouds and the tropical Pacific circulation: A coupled ocean–atmosphere GCM study. *J. Climate,* **9,** 1635–1645.

McAvaney, B., and Coauthors, 2001: Model evaluation. *Climate Change 2001: The Scientific Basis,* J. T. Houghton et al., Eds., Cambridge University Press, 471–523.

McWilliams, J. C., and F. Colas, 2010: Climate heat balance off western South America: Regional oceanic circulation and eddies. *CLIVAR Exchanges,* No. 53, International CLIVAR Project Office, Southampton, United Kingdom, 14–16.

Mechoso, C. R., and Coauthors, 1995: The seasonal cycle over the tropical Pacific in coupled ocean–atmosphere general circulation models. *Mon. Wea. Rev.,* **123,** 2825–2838.

Miller, R. L., 1997: Tropical thermostats and low cloud cover. *J. Climate,* **10,** 409–440.

Rossow, W. B., A. W. Walker, D. E. Beuschel, and M. D. Roiter, 1996: International Satellite Cloud Climatology Project (ISCCP) documentation of new cloud datasets. WMO Tech. Doc. 737, 115 pp.

Shinoda, T., and J. L. Lin, 2009: Interannual variability of the upper ocean in the southeast Pacific stratus cloud region. *J. Climate,* **22,** 5072–5088.

Simmons, A. J., and J. K. Gibson, 2002: The ERA-40 Project Plan. ECMWF ERA-40 Project Report Series 1, 63 pp.

Smith, R. D., J. K. Dukowicz, and R. C. Malone, 1992: Parallel ocean general circulation modeling. *Physica D,* **60,** 38–61.

Stephens, C., J. I. Antonov, T. P. Boyer, M. E. Conkright, R. A. Locarnini, T. D. O'Brien, and H. E. Garcia, 2002: *Temperature*. Vol. 1, *World Ocean Atlas 2001*, NOAA Atlas NESDIS 49, 169 pp.

Straneo, F., C. F. Moffat, R. A. Weller, and J. T. Farrar, 2010: Eddies in the southeast Pacific and their influence on the upper ocean. *Extended Abstracts, 2010 Fall Meeting,* San Francisco, CA, Amer. Geophys. Union, A54B-02. [Available online at http://adsabs.harvard.edu/abs/2010AGUFM.A54B..02S.]

Toniazzo, T., C. R. Mechoso, L. C. Shaffrey, and J. M. Slingo, 2010: Upper-ocean heat budget and ocean eddy transport in the south-east Pacific in a high-resolution coupled model. *Climate Dyn.,* **35,** 1309–1329, doi:10.1007/s00382-009-0703-8.

Uppala, S. M., and Coauthors, 2005: The ERA-40 Re-Analysis. *Quart. J. Roy. Meteor. Soc.,* **131,** 2961–3012.

Wittenberg, A. T., A. Rosati, N.-C. Lau, and J. J. Ploshay, 2006: GFDL's CM2 global coupled climate models. Part III: Tropical Pacific climate and ENSO. *J. Climate,* **19,** 698–722.

Wood, R., C. Bretherton, B. Huebert, C. R. Mechoso, and R. Weller, 2007: The VAMOS Ocean-Cloud-Atmosphere-Land Study (VOCALS): Improving understanding, model simulations, and prediction of the southeast Pacific climate system. Post-VOCALS-Rex Rep., 17 pp. [Available online at http://www.atmos.ucla.edu/~mechoso/Intro_Final.pdf.]

Xie, S.-P., 2004: The shape of continents, air-sea interaction, and the rising branch of the Hadley circulation. *The Hadley Circulation: Past, Present and Future,* H. F. Diaz and R. S. Bradley, Eds., Kluwer Academic Publishers, 121–152.

Yu, L., and R. A. Weller, 2007: Objectively analyzed air–sea heat fluxes for the global ice-free oceans (1981–2005). *Bull. Amer. Meteor. Soc.,* **88,** 527–539.

——, X. Jin, and R. A. Weller, 2008: Multidecade global flux datasets from the objectively analyzed air-sea fluxes (OAFlux) project: Latent and sensible heat fluxes, ocean evaporation, and related surface meteorological variables. Woods Hole Oceanographic Institution OAFlux Project Tech. Rep. OA-2008-01, 64 pp.

Zappa, C. J., J. T. Farrar, R. A. Weller, S. P. Bigorre, L. St Laurent, F. Straneo, and C. F. Moffat, cited 2010: Upper-ocean turbulence beneath the stratus cloud deck of the southeast Pacific. [Available online at http://adsabs.harvard.edu/abs/2010AGUFM.A51A0047Z.]

Zhang, Y., W. B. Rossow, A. A. Lacis, V. Oinas, and M. I. Mishchenko, 2004: Calculation of radiative fluxes from the surface to top of atmosphere based on ISCCP and other global data sets: Refinements of the radiative transfer model and the input data. *J. Geophys. Res.,* **109,** D19105, doi:10.1029/2003JD004457.

Zheng, Y., and B. S. Giese, 2009: Ocean heat transport in Simple Ocean Data Assimilation: Structure and mechanisms. *J. Geophys. Res.,* **114,** C11009, doi:10.1029/2008JC005190.

——, T. Shinoda, G. N. Kiladis, J.-L. Lin, E. J. Metzger, H. E. Hurlburt, and B. S. Giese, 2010: Upper-ocean processes under the stratus cloud deck in the southeast Pacific Ocean. *J. Phys. Oceanogr.,* **40,** 103–120.